Imaging the rapid yet transient accumulation of regulatory lipids, lipid kinases, and protein kinases during membrane fusion, at sites of exocytosis of MMP-9 in cancer cells

Dominique Stephens
Howard University
Tyrel Powell
Howard University
Justin Taraska
National Institutes of Health
Dinari Harris (dinari.harris@howard.edu)
Howard University

Research

Keywords: regulated exocytosis, fluorescence microscopy, PIP2 signaling, lipids, cancer

Posted Date: June 12th, 2020

DOI: https://doi.org/10.21203/rs.3.rs-34660/v1

Version of Record: A version of this preprint was published on August 23rd, 2020. See the published version at https://doi.org/10.1186/s12944-020-01374-9.

Imaging the rapid yet transient accumulation of regulatory lipids, lipid kinases, and protein kinases during membrane fusion, at sites of exocytosis of MMP-9 in cancer cells

Dominique C. Stephens, Tyrel W. Powell, Justin W. Taraska, and Dinari A. Harris*

[1]Department of Chemistry, Howard University, Washington, D.C. 20059, USA
[2]Laboratory of Molecular Biophysics, National Heart, Lung, and Blood Institute, National Institutes of Health, Bethesda, Maryland 20892, USA

Dinari A. Harris
525 College Street NW
Washington, DC 20059
dinari.harris@howard.edu
P: 1 202 806 6900

* To whom correspondence should be addressed. E-mail: dinari.harris@howard.edu

Keywords: regulated exocytosis; fluorescence microscopy, PIP2 signaling; lipids; cancer

Abstract

Background: The control of exocytosis is physiologically essential. *In vitro* SNARE proteins are sufficient to drive membrane fusion, but in cells there are additional proteins and lipids that work together to drive efficient, fast, and timely release of secretory vesicle cargo. Growing evidence suggests that regulatory lipids act as important lipid signals and regulate various biological processes including exocytosis. Though functional roles of many of these regulatory lipids has been linked to exocytosis, the dynamic behavior of these lipids during membrane fusion at sites of exocytosis in cell culture remains unknown.

Methods: We used total internal reflection fluorescence microscopy (TIRF) to observe the spatial organization and temporal dynamics of several lipids, and accessory proteins, like lipid kinases and protein kinases, in the form of protein kinase C (PRKC) relative to single sites of exocytosis of MMP-9 in living MCF-7 cancer cells.

Results: After stimulating exocytosis with PMA, we observed a transient accumulation of the regulatory lipids (*e.g.* PIP, PIP2, and DAG), lipid kinases (*e.g.* PI4K2B, PI4K3A, and PIP5KA), and protein kinases (*e.g.* PRKCA and PRKCE) at exocytic sites centered on the time of membrane fusion, before rapidly diffusing away from the fusion sites. Additionally, the synthesis of these regulatory lipids, degradation of these lipids, and the downstream effectors activated by these lipids, are also achieved by the recruitment and accumulation of key enzymes at exocytic sites (during the moment of cargo release), including lipid kinases, protein kinases, and phospholipases that facilitate membrane fusion and exocytosis of MMP-9.

Conclusions: This work suggests that these regulatory lipids and associated effector proteins are locally synthesized and/or recruited to exocytic sites, during the time of membrane fusion and

cargo release, and their enrichment at fusion sites serves as an important spatial and temporal organizing "element" defining individual exocytic sites.

Background

Exocytosis is a fundamental behavior, ubiquitous across eukaryotes and a variety of cell types. During exocytosis, vesicles fuse with the plasma membrane and result in secretion of biomolecules (vesicle cargo) to the outside of cells. This important mode of cellular communication can affect a variety of physiological processes, including polarized growth and motility [1, 2], cancer progression [3-5], and diabetes [6]. As it relates to cancer, defects in exocytosis have been implicated in many cancer types and are generally attributed to dysregulation in proteins involved in the discrete steps of exocytosis. Cancer progression relies, in part, on exocytosis to secrete a variety of protein factors, including growth factors, cytokines, proteases, and exosomes for establishment of tumor growth. During cancer progression, up-regulation of trafficking and secretion of several proteolytic enzymes, known as matrix metalloproteinases, MMPs, are responsible for degrading the extracellular matrix (ECM). This degradation by these proteases is a necessary step in tumor progression and metastasis.

Metastasis is a complex multicellular process that involves the dissemination of cancer cells through a series of sequential steps [7, 8]. During metastasis, the tumor migrates from the primary site to colonize distant (secondary) sites and represents the most common cause of cancer death. During metastasis, the ECM is degraded by the matrix-degrading proteins, MMPs, which are secreted by cells as a result of precisely organized intracellular cell signaling events. These MMPs rely on cells that utilize exocytosis to deliver secretory vesicles containing these proteases to the plasma membrane for subsequent release of the vesicle-associated cargo proteins to the outside of the cell. Therefore, MMPs play an important role in cancer progression by altering cell invasion, migration, metastasis, and tumorigenesis [7, 9-11]. Because of their important role in ECM degradation, MMPs have often been used as major biological markers of metastasis and acquisition of metastatic traits in cancer cells. Several studies indicate that increased expression of MMPs correlates with aggressive forms of several cancers, including colorectal, breast, ovarian, and melanoma [12-15]. Furthermore, this increased expression of several MMPs, including MMP-9, MMP-2, and MT1-MMP (*i.e.* MMP-14), are secreted by a variety of metastatic cancer cells to aid in ECM degradation [16, 17]. Therefore, it is clear that the release of MMPs depends on exocytosis associated with a variety of cancer cells.

During exocytosis, cells use more than twenty-five different proteins and an unknown number of lipids [18], participating in a cascade of protein-protein and lipid-protein interactions, and lipid signaling leading to the externalization of the secretory vesicle cargo molecules [19]. The minimal machinery required for fusion is a complex of three proteins, syntaxins, synaptosomal-associated proteins (SNAPs), and vesicle-associated proteins (VAMPs), collectively called the soluble N-ethylmaleimide–sensitive factor attachment protein receptors (SNAREs)[18, 20, 21]. This complex of proteins coil together to pull the plasma membrane and vesicle membrane into close apposition to drive fusion. For example, VAMP2, SNAP25, and syntaxin-1 were identified in brain tissue, where they mediate synaptic vesicle fusion and neurotransmitter release [20]. While VAMP3, SNAP23, and synatxin-13 were found to be involved in exocytosis of MMP-9 and MMP-2, degradation of the ECM, and subsequent cell invasion in fibrosarcoma cells [22].

Although the three SNARE proteins represent the minimal fusion machinery, fusion mediated by SNAREs only is relatively slow and uncoordinated. Therefore, though the SNAREs

are sufficient to induce membrane fusion *in vitro*, there are dozens of other accessory proteins and lipids that assemble together with the SNAREs to accelerate and regulate exocytosis in cells [18, 23]. The additional biomolecules essentially help to spatially and temporally coordinate the distinct steps associated with secretory vesicle fusion and exocytosis. Moreover, the SNAREs and the additional protein and lipid factors help to provide spatial and temporal cues or spatiotemporal organization associated with sites of secretory vesicle fusion (*i.e.* exocytic sites). The role of spatial and temporal organization at exocytic sites has been generally shown to occur through membrane specialization or organized spatial regions that have elevated levels of these factors at exocytic sites [24]. Specifically, the SNAREs, accessory proteins, and lipids form distinct organizing "elements" near the cell membrane, which interact with components of secretory vesicles and help facilitate exocytosis in cells. Fundamentally, these organizing "elements" can be grouped into three distinct classes and include: (1) specialized scaffolding proteins; (2) specialized lipids; and (3) the actin cytoskeleton network proteins [24].

The role of specialized lipids has become of increasing importance and overwhelming evidence suggests that specialized lipids, including regulatory lipids and other bioactive lipids, act as lipid-signaling mediators and affect a variety of cellular functions (*e.g.* signaling and regulation) [25], like the sequential stages underlying exocytosis (*e.g.* secretory vesicle trafficking, docking, priming, vesicle fusion, and recapture) [19]. The most notable of specialized lipids is the regulatory lipid, phosphatidylinositol-4,5-biphosphate (PI4,5P or PIP2) [26, 27, 28F148, 29, 30], which is a prerequisite for Ca^{2+}-dependent exocytosis [31], coordinates trafficking of secretory vesicles to their docking sites on the plasma membrane [32], and primes secretory vesicles for exocytosis, by recruiting accessory proteins and interacting with key components of the exocytic machinery (*e.g.* SNARE proteins) [33]. Additionally, the major upstream lipid precursor of PIP2 synthesis, phosphatidylinositol 4-phosphate (PI4P or PIP) is another distinct phosphoinositide (PI) lipid species, which regulates exocytosis by promoting docking of specific subpopulations of exocytic vesicles with the plasma membrane [34]. While the downstream degradation product of PIP2 hydrolysis, diacylglycerol (DAG) promotes exocytosis by recruiting vesicles to the immediate releasable pool through regulation of the vesicle priming protein, Munc13-1, in neuroendocrine cells [35].

The regulatory lipid, DAG has two possible fates, either phosphorylation to become the bioactive lipid, phosphatic acid (PA) or activation of protein kinase C (PRKC) via allosteric modification. Both downstream cellular fates have been functionally linked to exocytosis. PA can recruit proteins, like the SNAREs, thereby facilitating priming and vesicle fusion [36-38]. PRKCs are critical regulators of exocytosis through phosphorylation of distinct protein targets effecting or regulating the exocytotic machinery, including SNAP-25 and Munc18 [39-44]. The interconversion of these various distinct specialized lipids, as well as, downstream activation by DAG is achieved by specific lipid kinases, phospholipases, phosphatases, and protein kinases [45, 46]. Furthermore, these effector proteins have also been found to promote distinct steps involved in exocytosis [47-49] and suggests that local synthesis and degradation of these specific lipid species is achieved through the specific accumulation of these effector proteins at sites of membrane fusion and exocytosis [24, 27, 45, 50-52]. Overall, this implies that PIP2-mediated signaling: (1) is an important signal transduction pathway, involving a cascade of specialized lipids, and a variety of effector proteins, that are functionally linked to exocytosis; and (2) involves specialized lipids that possibly accumulate in defined microdomain regions, with some spatial and temporal patterning, in order to recruit effector proteins and promote exocytosis.

More and more, total internal reflection fluorescence (TIRF) has been utilized to image the spatiotemporal organization and dynamics associated with exocytosis in a variety of cellular contexts, including: (1) exocytosis involved in neurite elongation [53]; (2) exocytosis associated with cytoskeleton rearrangements and the formation of membrane fusion "hotspots" [54]; (3) viral exocytosis [55]; (4) microvesicles exocytosis [56]; (5) dense core vesicle (DCV) exocytosis [57] and; (6) secretory vesicle exocytosis [58]. We previously showed using two-color TIRF that it was possible to study the spatiotemporal patterning and dynamic behavior of several red fluorescently-labeled Rab GTPases, Rab effector proteins, and SNARE proteins (organizing "element #1; specialized scaffolding proteins) during regulated exocytosis of MMP-9, at individual membrane fusion sites or exocytic sites in MCF-7 adenocarcinoma cancer cells [58]. We found that many of these proteins stably assembled on docked secretory vesicles before exocytosis, however, at the moment of fusion, all of these components quickly diffused away and were lost from the exocytic site.

Here, to visualize exocytic vesicle fusion, we again exploited two-color TIRF microscopy to image the spatiotemporal organization and dynamics associated with specialized lipids (organizing "element" #2) and effector proteins on exocytosis of MMP-9 from MCF-7 breast cancer cells. To this end, we relied on the use of red fluorescently-tagged lipid-binding sensor proteins, with known specificity for single distinct lipids [59-63], to monitor the dynamics of several specialized lipids at sites of exocytosis of green fluorescently-tagged MMP-9. After stimulating exocytosis, using the known tumor promotor drug, phorbol myristate acetate (PMA), we observe a transient accumulation of the regulatory lipids, PIP2 and DAG, at exocytic sites centered at the time of membrane fusion and only lasting a few seconds. Also, we observe a concomitant recruitment of distinct lipid kinases and protein kinases (*i.e.* PRKCs) with kinetics broadly similar to PIP and DAG. This approach has allowed us to systematically map the dynamic behavior of lipids and proteins associated with PIP2-mediated signaling, at individual sites of exocytosis of MMP-9 in cancer cells. More importantly, spatiotemporal mapping and dynamic behavior of the regulatory lipids at sites of exocytosis in MCF-7 cells further establishes lipids as an important organizing "element" defining sites of fusion and regulated exocytosis in a variety of cell types.

Methods

Plasmids. Most plasmids were obtained fused to fluorescent proteins (*e.g.* EGFP, mCherry, RFP, or mTuruqoise2) and when necessary mCherry was replaced for the fluorescent proteins, usually EGFP in order to conduct two-color TIRF. Otherwise fusions were constructed from plasmids using either mCherry-N1 or mCherry-C1 as follows. MMP9-GFP (pEGFP-N1-MMP9) was a gift from Rene Harrison (University of Toronto, Toronto, ON). *Lipid sensors.* PIP2-sensor (GFP-C1-PLCdelta-PH, addgene #21179) [63]; DAG-sensor (GFP-N2-PRKCdelta-C1, addgene #21216) [62]; PIP-sensor ((PIP^{P4M}; mCherry-P4M-SidM; addgene #51471) [64]; PIP-sensor ((PIP^{Osh}), pRS406-PHO5-GFP-2xOsh2 PH domain (short), addgene #58829); PA-sensor (Raf1-mCherry generated from pDONR223-Raf1, addgene #23832) [65]; farnesylated-anchor (mCherry-Farnesyl-5, addgene #5505. *Lipid kinases.* PI4K3A (mTq2-PI4K3A), PI4K3B (GFP-PI4K3B), PI4K2A (PI4K2A-GFP), and PI4K2B (PI4K2B-GFP) were gifts from T. Balla, National Institutes of Health, Bethesda, MD) [64]; PIP5KA (mCherry-PIP5Kα) and PIP5KB (mCherry-PIP5Kβ) were gifts from S. Schmid, UT Southwestern Medical Center, Dallas, TX) [66]; PIP5KG (mCherry-PIP5K1c generated from DNASU: HsCD00000979). *Protein kinases.* PRKCA

(PRKCalpha-mCherry generated from PRKCalpha WT, addgene #211232), PRKCB (PRKCbeta-mCherry generated from PRKCbeta II, human), PRKCG (PRKCgamma-mCherry generated from pENTR-PRKCG, addgene #16180), PRKCD (PRKCdelta-mCherry generated from PRKCdelta WT, addgene #16386), PRKCE (PRKCepsilon-mCherry generated from FLAG-PRKCepsilon, addgene #10795), and PRKCZ (PRKCzeta-mCherry) were gifts from J. Taraska, National Institute of Health, Bethesda, MD); *Rab27 GTPases and prenylation mutants.* GFP-C1-Rab27a, GFP-C1-Rab27b, GFP-C1-Rab27a (GER), and GFP-C1-Rab27b (GER) were gifts from W. Westbroek, National Institute of Health, Bethesda, MD).

Cell culture and transfection. MCF-7 cells were maintained in Dulbecco's modified Eagles medium (DMEM) without phenol red (10% fetal bovine serum, 1% pen-strep, 11.1 mM glucose, 10 mM HEPES, 2 mM glutamine, 1 mM pyruvate) at 37°C at 5% CO_2. For experiments cells were plated on 25 mm collagen-coated coverslips. Cells were transfected using 1 μg of each plasmid with Lipofectamine 2000 according to the manufacturer's instructions and imaged 24-48 hours post-transfection. All imaging was performed at 28°C in imaging buffer (10 mM HEPES, 130 mM NaCl, 2.8 mM KCl, 5 mM $CaCl_2$, 1 mM $MgCl_2$, 10 mM glucose at pH 7.4). Exocytosis was stimulated by serum-starving transfected cells for 1 h followed by 30 min induction with 500 nM PMA prior to imaging. Chemicals were from Sigma-Aldrich, cell culture reagents and Lipofectamine from Life Technologies, and fixatives from Electron Microscopy Sciences.

TIRF Microscopy. TIRF microscopy was performed as previously described [57]. Briefly an inverted fluorescent microscope (IX-81; Olympus, Center Valley, PA) with a 100X/1.45 numerical aperture objective (Olympus) was used for TIRF imaging. Fluorescence was excited alternatively with 488 nm or 561 nm laser lines that were combined and passed through a 488/561DM filter cube (Semrock). Emission was spectrally separated using a 565DCXR dichroic mirror and projected side-by-side on an EM-CCD camera (DU 897; Andor) with a DualView image splitter (Photometrics, Tucson, AZ) containing 525Q/50 and 605Q/55 filters. The green and red images were superimposed in post-processing by acquiring an image of 100 nm yellow-green beads (Invitrogen) that were visible in both channels, mapping the position of six beads in both channels, and then superimposing the channels using projective image transform. This protocol was performed each day and the image transform was used to superimpose cell images. Images were acquired with IQ2 software (Andor) successively in the green then red channels with an exposure time of 500 ms and a 500 ms pause between pairs of images. Pixel size was 160 nm.

Structured Illumination Microscopy. TIRF-SIM imaging was performed on a DeltaVision OMX SR Structured Illumination. An inverted microscope is used with a spatial light modulator (SLM) that diffracts the beam using multiple grating patterns. In this system a 100X/1.49NA oil immersion objective lens is used with 488 nm (GFP) and 561 nm (mCherry) excitation and passed through a multi-band dichroic mirror (DM4). Red and green images were superimposed during processing using OMX SR task builder.

Image Analysis. All analysis was performed using custom Matlab scripts and ImageJ. Correlation analysis was performed as previously described [67]. All of the local maxima above a user-defined threshold and >2 μm away from the edge of the cell boundary were identified in each whole-cell green image (MMP9-GFP). Each local maximum was centered in a 4 μm × 4 μm cropped region. These cropped regions from several cells were each normalized to the brightest pixel and averaged

together. The regions corresponding to the green local maxima were also excised from the red images, normalized to the brightest pixel, and averaged together. In each average red image, 12 radial line scans were taken and averaged together. Randomly selected regions equal in number to the excised regions were processed in the same way. The average random line scan was then subtracted from the average red image line scan to account for background intensity statistics. Peak height for each construct was determined by measuring the maximum intensity difference between the first point (center of the image) and all other points in the averaged scan. Smaller 1.0 μm × 1.0 μm cropped, vesicle-centered red/green regions were used to calculate Pearson's *c* for each green peak:

$$c = \frac{\sum_{i=1}^{n}(\mathrm{Gi} - G)(\mathrm{Ri} - R)}{\sqrt{\sum_{i=1}^{n}(\mathrm{Gi} - G)}\sqrt{\sum_{i=1}^{n}(\mathrm{Ri} - R)}}$$

where G_i and R_i represent pixel intensities in the two channels and G and R indicates average pixel intensity. The region size was chosen based on the spacing of secretory vesicles in an attempt to capture only one structure per correlation region on average. Correlations were then averaged together, yielding an average C for each construct. Correlation values were calculated between peak-centered green excised regions and randomly selected red regions as well.

Exocytic events were analyzed by hand-selecting event coordinates and stack position in the green channel in ImageJ. Matlab scripts extracted a raw intensity mean (F_{center}) from a 480 nm square box centered on the coordinates and a mean background value from a 1440 nm square surround area ($F_{surround}$); this was performed for both channels. The traces were then temporally aligned to the frame before the maximum intensity decrease of the MMP9-GFP channel (t=0 in our trajectories). We aligned to the maximum intensity decrease because this was the most robust feature of MMP9-GFP signal at exocytic events. At the time resolution used here, the transient brightening of MMP9-GFP is always observed followed by the rapid decrease of fluorescence intensity in all traces. Individual trajectories were background subtracted and normalized over 0 to 1 by:

$$Normalized\ fluor. = \frac{((F_{center} - F_{surround}) - F_{min})}{F_{max} - F_{min}}$$

where F_{min} is the minimum fluorescence intensity over the F_{center} background-subtracted trace and F_{max} is the maximum. Average trajectories and standard errors were calculated from the normalized trajectories.

For all correlation analysis and analysis of exocytic events, 15 cells were imaged from cotransfections with the MMP-GFP and a red fluorescently-labeled protein. For these experiments, a single coverslip with cells cotransfected with MMP9-GFP and a red-labeled protein were imaged.

Western blotting. For detection of phosphorylated Rab protein (Rabphilin), cells were treated with and without PMA simultaneously in separate culture flasks. Cells were harvested, pelleted, and lysed with CHAPS Stock Solution 0.25% [w/v] in PhosphoProtein Lysis Buffer, with 1 complete protease inhibitor and Benzonase® Nuclease. Then incubated for 30 min on ice with intermittent vortexing. The cell lysate was centrifuged at 10,000 x g and 4°C for 30 min. Supernatant was harvested and the protein concentration determined. The protein concentration was adjusted to 0.1 mg/ml. The adjusted proteins were added to the PhosphoProtein Purification Column. Using PhosphoProtein Elution buffer, the isolated phosphoproteins were collected, and

concentration determined. Conditioned media phospho lysate protein content was quantified with a bicinchoninic acid assay (BCA-1; Sigma-Aldrich), and 10 μg of protein was loaded per lane on a 10–20% Tris-Glycine Novex gel (Invitrogen). The gel was transferred to a polyvinylidene fluoride membrane and blocked in 10% Omniblock in Tris-buffered saline with 0.2% Tween-20 1hr at room temperature. Blots were incubated using Rabphilin 3A (Ser234) antibody overnight at 4ºC, washed, and incubated in secondary antibody (anti-mouse, 1:2000). Followed by extensive washing and treatment with enhanced chemiluminescence kit and exposure to film. The anti-phospho Rabphilin 3A (Ser234) antibody was purchased from PhosphoSolutions (#p1553-234). All bands from western blot were quantified using ImageJ software (NIH, Bethesda, MD). For quantification, all band intensities were measure and averaged from four separate experiments.

Results

Systematic spatial mapping of specialized lipids associated with secretory vesicles containing MMP-9 at exocytic sites

We used MCF-7 breast cancer cells, which can be used as a model system for regulated exocytosis of MMP-9, to probe the lipid environment of secretory vesicles containing MMP-9 and their subsequent exocytosis in living cells. To visualize secretory vesicles, we transiently transfected MCF-7 cells with a secretory vesicle cargo marker, matrix metalloproteinase 9-GFP (MMP9-GFP), which is packaged into the secretory vesicles in cancer cells [22]. When imaged with TIRF in MCF-7 cells, we observed a field of diffraction limited, punctate spots that appeared to be mostly immobilized at the plasma membrane similarly to what has been previously seen [22, 58]. These spots correspond to small and spherically shaped (˜120 nm diameter) secretory vesicles when imaged with electron microscopy [58]. To determine the spatial arrangement of lipids at secretory vesicles containing MMP-9, we used two-color TIRF microscopy to image the colocalization of these vesicles with various specialized lipids in living MCF-7 cells. For colocalization experiments and to probe the dynamic lipid environment at secretory vesicles and exocytic sites, we used MMP9-GFP cotransfected with a specific lipid sensor fused to a red fluorescent protein (mainly mCherry). Specific lipid species are visualized using lipid sensors, which are fluorescent proteins fused to protein domains with known specificity for single lipids. Lipid sensors are protein domains from lipid binding proteins, like pleckstrin homology (PH) domain from phospholipase C (PLC), which is well-characterized and has specific binding to a particular lipid species [59]. These lipid sensors are routinely used to image the endogenous lipid distribution in living cells [62, 63] and we are using them to image the spatial organization and dynamic behavior of these specialized lipids at exocytic sites of MMP-9. We used a variety of available and widely accepted lipid sensors to determine colocalization with secretory vesicles containing MMP-9.

Using a well-established TIRF-based imaging screen [56-58, 67] and following cotransfection of MCF-7 cells with MMP9-GFP and mCherry-tagged lipid sensors, we measured the steady-state colocalization or relative association between docked secretory vesicles and a panel of lipid sensors (Figure 1). Imaging revealed that docked secretory vesicles containing MMP9-GFP were detected as punctate structures, while correlation analysis showed broad labeling and distribution of lipid sensors across the plasma membrane. None of the lipid sensors tested appeared to be solely or highly enriched at docked secretory vesicles containing MMP9-GFP. Figure 1 shows two separate lipid sensors tested, including the PIP2-sensor (Figure 1A) and the DAG-sensor (Figure 1B). The PIP2-sensor used is a fusion of the PH domain of phospholipase

C δ1 (PLC-δ1) with the red-fluorescent protein, mCherry (mCherry-C1-PLCdelta-PH) [63] and the DAG-sensor is a fusion of the C1 domain of PRKCδ with mCherry (C1-PRKCdelta-mCherry). Both the PIP-sensor and the DAG-sensor recognize only one distinct specific lipid species and therefore represents suitable *in vivo* indicators of that lipid species. Similar to previous reports of these lipid-sensor [62, 63], we observed a heterogenous distribution of both lipids sensors with more ubiquitous expression across the plasma membrane and punctate localization associated with docked membrane-bound secretory vesicles in MCF-7 cells.

Correlation values were determined for the red-labeled lipid sensors and associated effector proteins relative to secretory vesicles containing MMP9-GFP and subsequently separated in four categories (highly correlated, moderately correlated, weakly correlated, and non-specifically/not associated) as similarly reported for the same TIRF based imaging method [57, 58, 67]. In general, correlation values of red-labeled proteins associated with secretory vesicles containing MMP-9 above >0.20 represent colocalized proteins (highly, moderately, and weakly correlated) and below <0.20 represent correlation values of nonspecifically or not associated with secretory vesicles containing MMP-9. This 0.20 cutoff has previously been used to identify nonspecific or not associated proteins, using identical TIRF based screen [57, 58]. The lipid sensors tested showed a range of low correlation values (C=0.02-0.31) with MMP-9 (Figure 1C) and do not appear to be statistically different than the relatively nonspecific cytosolic and membrane-anchored probes tested (controls; cytoplasmic-mCherry and farnesyl-mCherry). Though we observed many secretory vesicles containing MMP9-GFP colocalized with the lipid sensors, our correlation values are relatively low because of the overwhelming number of MMP9-GFP secretory vesicles that did not show punctate staining with the lipid-sensors. As a positive control, we determined the correlation value for MMP9-mCherry to be 0.67, which represents the highest correlated protein with MMP9-GFP [58]. Correlation values ranging from 0.20-0.34 represent weakly colocalized proteins and lipid sensors, and include PIP2, DAG, PIP^{Osh2}, PIP5KA, PIP5KB, PRKCB, PRKCG and PRKCD, while values below 0.20, include PIP^{P4M}, PA, PI4K2A, PI4K2B, PI4K3A, PI4K3B, DGKA, DGKD, DGKG, PIP5KG, PRKCA, PRKCE and PRKCZ (Figure 1C). Collectively this represents several lipids associated with the PIP2-mediated signaling pathway, as well as, several lipid kinase isoforms and protein kinase C isoforms that are responsible for the synthesis of these lipids or are downstream effectors of these lipids. Overall, this spatial patterning data suggests that the majority of specialized lipids, lipid kinases, and protein kinases are only weakly or nonspecifically/not associated with docked secretory vesicles containing MMP-9.

This imaging-based screening method relies on transient transfection of cells with fluorescently tagged proteins. This method enabled rapid determination of the spatial patterning and dynamic temporal behavior associated with subset of lipid sensors and effector proteins (*e.g.* lipid and protein kinases) at exocytic sites of MMP-9, which would not have been feasible using lower-throughput methods such as genome-engineered cell lines [68, 69]. Furthermore, transient expression allowed us to visualize patterning and dynamics that might otherwise be difficult to detect at lower expression levels under either endogenous or lower-expression promotor control. To test for possible overexpression effects on our colocalization analysis, we confirmed by using all of our lipid sensor and effector proteins that there was no relationship between expression and correlation values (data not shown). Similar effects were also seen using a neuronal secretory granule marker in both PC12 cells [67] and INS-1 cells [57].

PMA-induced exocytosis of MMP-9 accompanied by transient recruitment of regulatory lipids to exocytic sites

Next, we characterized the temporal dynamics associated with the lipid environment at fusion sites, following regulated exocytosis of MMP-9. To promote secretion of MMP-9 from secretory vesicles, we stimulated MCF-7 cells using the tumor promotor, PMA [70], which reproducibly triggers robust exocytosis of MMP-9 in these cells. Using two-color TIRF, we imaged the behavior of red fluorescently-tagged lipid sensors (red channel) at fusion sites, during PMA-stimulated exocytosis of MMP9-GFP (green channel). We identified exocytic sites or fusion events, as a sudden sharp increase (or spike) in MMP9-GFP from a docked secretory vesicle, followed by a rapid fluorescence decay as MMP-9 diffuses away from the site of exocytosis. This dynamic behavior observed using TIRF is a hallmark of exocytosis and has been observed at single sites of exocytosis, including the release of: (1) NPY from dense core vesicles (DCVs) in endocrine INS-1 cells [57]; (2) vesicular acetylcholine transporter from small synaptic-like microvesicles (SLMV) in PC12 cells [56]; and (3) MMP-9 from secretory vesicles in MCF-7 cells [58]. By monitoring the decay kinetics, quantitating the fluorescence intensity changes (in both the green and red channels) that occurred at individual exocytic sites of MMP-9, and averaging fusions events from many MCF-7 cells, we were able to produce an average time-dependent fluorescence change from both channels.

We began by examining the temporal dynamics of regulatory lipids at individual sites of exocytosis of MMP-9 in MCF-7 cells. In regulated exocytosis, the importance of regulatory lipids, PIP2 and DAG, are well documented as secondary messengers involved in several cellular signaling pathways [50], including the distinct steps of regulated exocytosis [28, 31, 51, 59, 71];[35, 44, 46, 62, 63, 72, 73]. PIP2 is an important recruiting factor, priming secretory vesicles for exocytosis, by interacting with several essential exocytic proteins [71]. DAG is another regulatory lipid implicated in controlling exocytosis and has been shown to increase stimulus-coupled secretion, by recruiting vesicles to the immediately releasable pool through the regulation of the vesicle priming protein Munc13-1 in neuroendocrine cells [35]. Because of the known roles and involvement of these regulatory lipids in exocytosis, we used two-color TIRF to observe the temporal dynamic fluorescence changes associated with either the PIP2-sensor or DAG-sensor (red channel), at sites of exocytosis of MMP9-GFP (green channel). To this end, we generated representative time-aligned snapshots and average quantitative analysis from exocytic fusion events of MMP9-GFP in the green channel (Figure 2A for PIP2-sensor and Figure 2C for DAG-sensor), and the corresponding region in the red channel for both PIP2-sensor (Figure 2B) and DAG-sensor (Figure 2D). We found that both regulatory lipid sensors are transiently enriched at sites of exocytosis of MMP-9, at the moment of fusion before diffusing away from exocytic sites (Figure 2B and 2D). Accumulation of both PIP2 and DAG at exocytic sites have broadly similar kinetics (*i.e.* sharp rise followed by slower decay) and suggests that enrichment of regulatory lipids occurs only at sites of membrane fusion and exocytosis of MMP-9. We did not observe any accumulation of the control lipid marker farneslyated-mCherry (a lipid-anchored protein), control mCherry protein, or the mutated PIP2-sensor, which is unable to bind PIP2 [63], at fusion events (Supplemental Figure 1).

Since DAG is generated directly from PIP2 hydrolysis by PLC, it suggests that the DAG might be locally synthesized at exocytic sites following recruitment and/or synthesis of PIP2 at these sites. Because the PIP2-sensor we used contains the PH domains from PLC [63], we predicted that exocytosis of MMP-9 would be altered in the presence of an inhibitor of PLC. We observed that inhibition of PLC stops exocytosis of MMP-9, following the addition of 10 μM of U-73122, a PLC inhibitor. There were no observable fusion events and no vesicle trafficking between docked sites, in the presence of the PLC inhibitor. This suggested that PLC inhibition

blocked local hydrolysis of PIP2 and DAG synthesis, and subsequent loss of MMP-9 release. It is worth noting that we cannot discount a non-specific effect that might be caused by the inhibition. Overall, our TIRF data suggest that regulatory lipids PIP2 and DAG, have dynamic temporal behavior at individual sites of exocytosis of MMP-9 in MCF-7 cells, and suggest that the specialized lipids are transiently accumulated at these spatial positions at precisely the moment of fusion.

PMA-induced exocytosis of MMP-9 accompanied by accumulation of specialized lipids and lipid kinases to exocytic sites

Since the regulatory lipid, PIP2 is transiently enriched at exocytic sites during the release of MMP-9, we wanted to examine the role of the upstream lipid and lipid kinases involved in the pathway of PIP2 synthesis. PIP2 can be synthesized through the action of two distinct but related phosphoinositide kinases (*i.e.* lipid kinases) [74]. First, the phosphorylation of the lipid, phosphatidylinositol to phosphatidylinositol 4-phosphate, PI4P (or PIP), occurs and represents the first committed step in the generation of PIP2 and is catalyzed by the lipid kinase, PI4-kinase, PI4K. Second, the lipid, PI4P (or PIP) undergoes another phosphorylation to phosphatidylinositol-4,5-bisphosphate, PI45P (or PIP2), by the lipid kinase, phosphatidylinositol 4-phosphate 5-kinase, PIP5K.

We tested the dynamics associated with two different PIP lipid sensors, as well as, four different PI4K isoforms, including PI4K2A, PI4K2B, PI4K3A, PI4K3B, at exocytic sites of MMP-9. We used two different PIP lipid sensors to monitor dynamics during fusion and exocytosis of MMP-9. One of the PIP lipid sensors was derived from the PI4P binding of the SidM (P4M) domain of the secreted effector protein SidM from the bacterial pathogen *Legionella pneumophila* [64]. We observed that during exocytosis of MMP-9, there is a transient accumulation of PIP^{P4M} around the time of fusion, followed by rapid diffusion decay away from the membrane upon vesicle cargo release (Figure 3A). The second PI4P lipid sensor was derived from the PH domain from oxysterol (Osh) binding protein [75, 76] and can recognize PI4P, similar to P4M, but represents an older and far less sensitive probe for plasma membrane PI4P. We observed using this PIP lipid sensor, PIP^{Osh}, a decrease in fluorescence over time following the exocytosis of MMP-9 (Figure 3B). It is worth noting that these differing findings with the varying PIP lipid sensors are consistent with reports of different PI4P binding domains probing distinct cellular populations [64]. Several reports suggest that the presence and activity of PI4K on synaptic vesicles or DCVs facilitates and promotes exocytosis [47-49]. Therefore, we also examined the dynamic behavior of several mCherry-tagged lipid kinases at exocytic sites of MMP-9, including four PI 4-kinase isoforms (*e.g.* PI4K2A, PI4K2B, PI4K3A, PI4K3B) [64]. Following stimulation with PMA, we observed a reproducible accumulation of both PI4K2A and PI4K2B following the moment of exocytosis of MMP-9. With PI4K2A, the fluorescence signal remained elevated at fusion sites for at least one minute after release (Figure 4A), while PI4K2B, the fluorescence signal only transiently accumulated post-exocytosis of MMP-9 (Figure 4B), and this brief accumulation following membrane fusion occurs consistently and reproducibly approximately five to ten seconds after the release of MMP-9. After stimulation with PMA, we observed a rapid, yet transient accumulation of PI4K3A (Figure 4C) during membrane fusion and exocytosis of MMP-9, similar to that observed with the PIP^{P4M} sensor. However, we observed no change in fluorescence around the moment of membrane fusion using PI4K3B (Figure 4D).

Since, we observed a transient accumulation of PIP2 at exocytic sites of MMP-9 (Figure 2B), we next tested the dynamic behavior of three different isoforms of PIP5K, including PIP5KA,

PIP5KB, and PIP5KG, responsible for the synthesis of PIP2. Evidence suggests a function of PIP5K in regulated exocytosis, as depletion of PIP5K from the plasma membrane caused the inhibition of DCV exocytosis and overexpression of PIP5K restored exocytosis [71]. Moreover, PIP5K is involved in Ca^{2+}-induced fusion with docked vesicles near the plasma membrane in the PC12 cells [77]. After stimulation with PMA, we observed differing dynamic behaviors with the various mCherry-tagged PIP5K isoforms, at exocytic sites of MMP-9. The PIP5KA showed decrease fluorescence over time following the exocytosis of MMP-9 (Figure 5A) and suggests this isoform is released from sites of secretory vesicle fusion after cargo release. We observed no exocytic events associated with MMP-9 release following cotransfection with PIP5KB, suggesting a possible inhibitory effect or overexpression effect from PIP5KB on regulated exocytosis. The PIP5KG sensor exhibited the most dynamic temporal changes at exocytic sites, showing transient accumulation prior to fusion and exocytosis of MMP-9 (Figure 5B). We observed a rapid (and reproducible) accumulation of PIP5KG approximately five seconds before the moment of membrane fusion. These results on the dynamic behavior associated with the various lipid kinases, like PI4K and PIP5K, and the lipid precursor, PI4P (or PIP), suggests these biomolecules are accumulated at sites of exocytosis of MMP-9, during or around the time of membrane fusion. Their accumulation at exocytic sites before, during, or after exocytosis of MMP-9 at fusion sites: (1) reiterates the idea that many specialized lipids (*e.g.* PIP, PIP2, and DAG) are locally synthesized at exocytic sites with the help of several lipid kinases (also enriched at fusion sites); (2) reinforces the role of lipids as organizing "elements" identifying sites of fusion and cargo release; and (3) underscores the important role that the lipid precursors of PIP2 and the upstream effectors involved in PIP2 synthesis have on regulated exocytosis of MMP-9 in MCF-7 cells.

Enrichment of protein kinase C isoforms at exocytic sites, around the moment of fusion, following PMA-induced exocytosis of MMP-9

Because of the accumulation of DAG at exocytic sites during the PMA-induced release of MMP-9, we wanted to examine the role of PRKCs during these fusion events. PRKC function is commonly examined using PMA, because it is a potent DAG analogue that acts as a PRKC activator [78-81]. Moreover, DAG stimulates exocytosis through activation of PRKCs, downstream signaling proteins involved in membrane trafficking and exocytosis [43, 73], via phosphorylation of key secretory proteins, such as SNAP25 [82, 83], synaptotagmins [84, 85], and MUNC18 [39, 86]. We examined the temporal dynamics of the various PRKC isoforms from the three major groups, including conventional (alpha, beta, and gamma), novel (delta and epsilon), and atypical (zeta), at exocytic sites of MMP-9 in MCF-7. Following stimulation with PMA, we observed a rapid, yet transient accumulation of PRKCA and PRKCE at sites of exocytosis (Figure 6A & 6E). The decay kinetics associated with both isoforms show broad similarity to those observed for the DAG-sensor. While PRKCB and PRKCG do not show accumulation at the moment of fusion, both isoforms still laterally diffuse away from the exocytic site following fusion (Figure 6B & 6C), as suggested by their decrease in fluorescence at 0 seconds (time). Lastly, we did not observe any changes in fluorescence during fusion events with the PRKCD and PRKCZ (Figure 6D & 6F). Overall, this data suggests that the PRKC isoforms, PRKCA and PRKCE, are specifically accumulated at exocytic sites during membrane fusion, following PMA-induced exocytosis in MCF-7 cells and this enrichment occurs transiently at the moment of fusion and release of MMP-9. To further investigate the involvement of the various PRKC isoforms in the release of MMP-9, we cotransfected MCF-7 with MMP9-GFP and siRNAs against PRKCA, PRKCD, or PRKCE. Following the addition of PMA, cells transfected with siRNAs knocking

down PRKCD or PRKCE caused a significant reduction in the number of exocytic events occurring on average in each cell. Cells transfected in the absence of siRNAs showed on average >˜15 fusion events total per set of cells imaged, while knockdown of PRKCD or PRKCE resulted in one to two fusion events per set. Additionally, cells transfected with siRNAs against PRKCA showed no fusion events per cell. Altogether, our results suggest that several PRKC isoforms accumulate at exocytic sites involving the release of MMP-9 from MCF-7 cells.

Since our data suggested a role of several PRKC isoforms in regulated exocytosis of MMP-9 from MCF-7 cells, we wanted to identify a possible target of phosphorylation by the PRKCs. PRKCs have been shown to phosphorylate several key components associated with secretory vesicles and/or exocytic machinery at fusion sites, including Rabs (and Rab effector proteins) [87, 88], vesicle bound SNARE proteins [82, 83, 89], and MUNC18 [39, 86]. Although, over the years a few targets of phosphorylation by the PRKC proteins have been identified in the context of neuronal or neuronal-like cell lines, the majority of targets for regulation by phosphorylation *in vivo* in other secretory vesicle cell types are unknown. To compare western blots on cells following PMA-induction on uninduced cells, phosphoprotein specific antibodies targeting any of the secretory vesicle proteins and the exocytic machinery in non-neuronal MCF-7 cells would be needed. The lack of phosphoprotein specific antibodies left us with limited target options. However, Rabphilin 3A (Ser234) antibody was available and used to detect phosphorylation of a Rab effector protein known to have an association to exocytic machinery and is expressed in a variety of secretory vesicle cell types, including both neuronal and non-neuronal cells lines. We purified lysates that were either PMA-uninduced or PMA-induced using a phosphoprotein purification kit, followed by conducting western blots using anti-phospho Rabphilin 3A (Ser234) antibody, a probe specific for phosphorylated Rabphilin. We were not able to see enrichment of phosphorylated Rabphilin following purification using the phosphoprotein purification kit. This is likely because the purification results in large loss of proteins and subsequent lack of detection using the kit (Figure 7A). However, the western blots did show phosphorylated Rabphilin following PMA-induction in unpurified lysates. While blots using unpurified lysates from cells not induced with PMA revealed no visible band corresponding to phosphorylated Rabphilin 3A (Figure 7A). This result suggests that PRKC proteins possibly target Rab effectors proteins, which is consistent with previous studies showing different Rab proteins as targets for PRKC isozymes [88, 90-92]. Further work will be necessary to characterize this possible functional link of phosphorylated Rabphilin 3a and exocytosis, however, the western blot is consistent with a role of PRKC in regulated exocytosis in MCF-7 cells.

Although, we were unable to identify additional specific targets of the PRKC proteins in MCF-7, we hypothesized that any target of the PRKCs involved in exocytosis would require close proximity between PRKCs and secretory vesicle proteins at sites of PMA-induced exocytosis. We, therefore, used the super-resolution technique, TIRF-SIM (total internal refection fluorescence structured illumination microscopy) to determine the proximity (*i.e.* spatial positioning) of PRKCs to secretory vesicles containing MMP-9, following PMA-induction. TIRF-SIM has recently been used for high resolution imagining, improved spatial resolution, and enhanced resolution from live cell imaging to detect a variety of colocalizations and dynamic interactions between organelles or with the plasma membrane [93-95]. We observed vesicles containing MMP-9 colocalized strongly with the PRKCE isoforms (Figure 7B), following PMA stimulation. However, we observed no direct colocalization with PRKCA or PRKCG, following induction with PMA (data not shown). This is consistent with our dynamic imaging data suggesting that a PRKC specific isoform (*e.g.* PRKCE) may accumulate at exocytic sites and could potentially phosphorylate any number of

proteins associated with secretory vesicles containing MMP-9. We also examined the spatial positioning of PRKC isoforms with Rab27 GTPase isoforms (organizing "element #1; specialized scaffolding proteins), which revealed punctate localization and a close proximity of PRKCA and Rab27b (Figure 7D), following PMA induction. There was no punctate localization or close proximity associated with PRKCA and Rab27a (Figure 7C) with any isoform and we observed no direct localization with Rab27b and PRKCG and PRKCE (data not shown). This result implies that a PRKC specific isoform (*e.g.* PRKCA) is highly localized with the Rab27 GTPase specific isoform, Rab27b and suggests that the targets of phosphorylation might be associated with Rab27b-specific secretory vesicles.

Phosphatic acid showed no accumulation at exocytic sites, around the moment of fusion, during PMA-induced exocytosis of MMP-9

Various other lipids and their associated protein effectors are suspected to take part in regulated exocytosis, including phosphatidic acid, PA. PA has been found to be involved in exocytosis [45, 52], via the recruitment of proteins for vesicle fusion or priming events (such as SNAREs) and to facilitate efficient vesicle exocytosis [36-38]. Given our evidence of regulatory lipid turnover at exocytic sites, we examined the role of PA at exocytic sites. Because DAG is further metabolized to PA, via the activity of diacylglycerol kinase (DGK), we monitored the dynamics of DGKs and its downstream product, PA, at fusion sites, during PMA-induced exocytosis of MMP-9. We observed a small number of fusion events following overexpression of the PA-sensor (Raf1) and there was no change in fluorescence associated with the PA-sensor at exocytic sites during membrane fusion (Supplemental Figure 2A). Moreover, imaging the three different isoforms of DGK (alpha, delta, and gamma), we also observed only a few fusion events and no evidence of these proteins accumulating at sites of exocytosis during the moment of fusion (Supplemental Figure 2B-D). This suggests that PA and associated effector proteins, DGKs, display little temporal dynamics during exocytosis of MMP-9 at individual sites of fusion in MCF-7 cells. It is important to note that overexpression of the majority of the lipid sensors and effector proteins did not have an effect on the number of fusion events (*N*; see figure legends) examined per set, except for the PA-sensor and the DGK's which all showed reduced number of fusion events. This suggests that the overexpression of the majority of fluorescently-tagged lipid sensors and effector proteins tested do not affect membrane fusion events at exocytic sites. However, we cannot fully exclude the possibility that the native behavior of the lipid sensor or effector proteins could be modulated by expression levels or fluorescent tagging.

Mutations effecting prenylation (a lipid modifications) of Rab27 isoforms alter MMP-9 release dynamics at exocytic sites

We also examined the role of prenylation of Rab27 isoforms, Rab27a and Rab27b, at sites of exocytosis of MMP-9. Protein prenylation is a specific type of lipid modification made to some proteins, including Rab GTPases and involves the transfer of either geranylgeranyl or a farnesyl moiety to C-terminal cysteines on target proteins [96]. Geranylgeranyl modifications are important in mediating protein-protein interactions and protein-membrane interactions [97] and both Rab27 isoforms undergo geranylgeranylation [96]. We previously observed that both Rab27a and Rab27b, which are implicated in late-stage exocytosis, were localized to sites of exocytosis of MMP-9 and potentially act as scaffolding proteins (another type of organizing "element") at exocytic sites [58]. Consistent with previous observations reported for the overexpression of the constitutively active or dominant-negative mutations of the Rab27a and Rab27b isoforms, we

observed that mutations made to the geranylgeranyl region of both Rab27 also delayed decay kinetics associated with MMP-9 exocytosis. Fusion decay kinetics (with standard error) for the Rab27a mutants slowed by approximately four-fold from in $\tau = 1.3 \pm 0.0$ s (WT) to $\tau = 4.7 \pm 0.4$ s (prenylation) (Figure 8A), while Rab27b prenylation mutants slowed by approximately six-fold, from $\tau = 1.1 \pm 0.0$ s (WT) to $\tau = 6.2 \pm 0.3$ s (prenylation) (Figure 8C). We also examined the protein dynamics of the Rab27 isoform–specific prenylation mutants (red channel) at these sites of exocytosis of MMP-9. When Rab27a- and Rab27b-specific prenylation mutants were overexpressed in PMA-induced MCF-7 cells, we found localization to sites before fusion that diffuse away following exocytosis of MMP-9, like their WT counterparts (Figure 8B and 8D). Specifically, for the Rab27a- and Rab27b-specific prenylation mutations (Rab27a-Ger or Rab27b-Ger), we observed a weakened or smaller change in fluorescence decay following fusion, suggesting that they may not be lost from the site of fusion as fast as in WT. These results in both the green and red channels are consistent with the data reported with the constitutively active or dominant-negative versions of these Rab27 mutants previously reported [58]. Moreover, the temporal dynamics associated with the Rab27 isoforms (organizing "element" #1: scaffolding proteins) contrast significantly with the overall dynamic behavior associated with several specialized lipids (organizing "element"#2: lipids).

Figure 1: Representative TIRF images from the correlation analysis using lipid sensors tagged with a red-fluorescent protein associated with secretory vesicles, including images of MMP9-GFP, cotransfected with the: (A) PIP2-sensor; or (B) DAG-sensor. TIRF images from green channel of MMP9-GFP (left); red channel of either PIP2-mCherry or DAG-mCherry lipid sensor (middle); and merge from both green and red channel (right) from a MCF-7 cell. Scale bar, 10μm. Correlation analysis with MMP9-GFP measures colocalization with secretory vesicles in uninduced cells. Shown is the correlation analysis of 22 proteins, which include lipid sensors, lipid kinase isoforms, and protein kinase C isoforms (PRKCs) with MMP9-GFP–labeled secretory vesicles in MCF-7 cells (C). Cells are sorted based on their position in the lipid signaling cascade. Red boxes above 0.2 (referenced by the dotted line) indicate proteins associated with secretory vesicles, and boxes below 0.2 indicate proteins that are nonspecifically or not associated with secretory vesicles. The whiskers are the standard error (SE) and the × marks above and below each data set are the standard deviation (SD). For all correlation assays using two-color TIRF, 15 cells were imaged from cotransfections with the MMP-GFP and a red fluorescently labeled protein.

Figure 2: Gallery of representative TIRF images of MCF-7 cells transfected with MMP9-GFP and red fluorescent-labeled PIP2-sensor (A-D) and DAG-sensor (E-H). Shown is a fusion event in the green channel (A, E) and the corresponding region in the red channel for the PIP2-sensor (B) or DAG-sensor (F), following stimulation with PMA. Snapshots of the fusion event are at the indicated time-points. '0 s' is the manually identified first frame of brightening in the green channel. Circles (~1 μm diameter) represent regions used for intensity analysis. Average time-lapse traces of normalized fluorescence intensities for fusion events shown in the green (C & G) and red channels (D & H). Standard errors are plotted as (gray) areas around the average (green or red) trace. *N*=25 for PIP2 and 33 for DAG2. Dashed line marks the zero-time point that was generated from individual MMP9-GFP fusion event traces (green channel) and time aligned to the red channel. For all exocytosis assays using two-color TIRF, 15 cells were imaged from cotransfections with the MMP-GFP and a red fluorescently-labeled protein. A single coverslip with cells cotransfected with MMP9-GFP and a red-labeled protein were imaged.

Figure 3: Average time-lapse traces of normalized fluorescence intensities signal (dark line) of the red fluorescent-labeled PI4P- or PIP-sensors, including: (A) PIP^{P4M}, *N*=15; and (B) PIP^{Osh}, *N*=19 and the SE of the data is show in (gray) for all traces. Dashed line marks the zero-time point that was generated from individual MMP9-GFP fusion event traces (green channel) and time aligned to the red channel. Background-subtracted and normalized fluorescence intensity traces are shown for each protein.

Figure 4: Average time-lapse traces of normalized fluorescence intensities signal (dark line) of red fluorescent-labeled lipid kinase isoforms, including: (A) PI4K2A, *N*=11; (B) PI4K2B, *N*=24; (C) PI4K3A, *N*=21; and (D) PI4K3B, *N*=16 and the SE of the data in (gray) for all traces. Dashed line marks the zero-time point that was generated from individual MMP9-GFP fusion event traces (green channel) and time aligned to the red channel. Background-subtracted and normalized fluorescence intensity traces are shown for each protein.

Figure 5: Average time-lapse traces of normalized fluorescence intensities signal (dark line) of red fluorescent-labeled lipid kinase isoforms, including: (A) PIP5KA, *N*=23; and (B) PIP5KG, *N*=11 and the SE of the data in (gray) for all traces. Dashed line marks the zero-time point that was generated from individual MMP9-GFP fusion event traces (green channel) and time aligned to the red channel. Background-subtracted and normalized fluorescence intensity traces are shown for each protein.

Figure 6: Average time-lapse traces of normalized fluorescence intensities signal (dark line) of red fluorescent-labeled protein kinase C isoforms, including: (A) PRKCA, *N*=25; (B) PRKCB, *N*=16; (C) PRKCG, *N*=16; (D) PRKCD, *N*=13; (E) PRKCE, *N*=25; and (F) PRKCZ, *N*=5 and the SE of the data in (gray) for all traces. Dashed line marks the zero-time point that was generated from individual MMP9-GFP fusion event traces (green channel) and time aligned to the red channel. Background-subtracted and normalized fluorescence intensity traces are shown for each protein.

Figure 7: (A) Western blot, using unpurified lysates and various components, eluants versus concentrates, associated with phosphoprotein purification kit, for phospho-specific Rabphilin 3A (Ser234), without and with PMA-induction. Spatial organization, super resolution SIM images of PRKC isoforms with its potential phosphorylation targets during PMA induction. Shown on the left is the spatial arrangement of: (B) PRKCE with MMP9-GFP; (C) PRKCA with Rab27a; and (D) PRKCA with Rab27b. Shown on the right is the enlarged regions (boxes on left); same order as on the left.

Figure 8: (A) Average time-lapse decay profiles of normalized MMP-9 fluorescence intensities (green channel; top), co-expressed with Rab27a-WT, wild-type (solid black) and Rab27a-Ger (dashed gray). The average time-lapse decay profiles of the associated normalized Rab27a-WT and Rab27a-Ger mutant fluorescence intensities (red channel; bottom) in the same MCF-7 cells is also depicted. (B) Average time-lapse decay profiles of normalized MMP-9 fluorescence intensities (green channel; top), co-expressed with Rab27b-WT (solid black) and Rab27b-Ger (dashed gray). The average time-lapse decay profiles of the associated normalized Rab27b-WT and Rab27b-Ger mutant fluorescence intensities (red channel; bottom) in the same MCF-7 cells is

also depicted. Individual event traces were time-aligned to '0 s', which corresponds to the manually identified first frame of fusion.

Figure 9: A depiction of the PIP2-mediated signaling pathway on the exocytosis of MMP-9 in MCF-7 cells. Illustration shows a step associated with dynamic cascade of PIP2 formation and subsequent breakdown, and the lipid kinases and protein kinases associated with exocytic sites.

Supplemental Figure 1: Average time-lapse traces of normalized fluorescence intensities signal (dark line) of red fluorescent-labeled: (A) farneslyated-mCherry protein, *N*=34; (B) mCherry protein, *N*=30; and (C) mutated PIP2-sensor, *N*=17 and the SE of the data in (gray) for all traces. Dashed line marks the zero-time point that was generated from individual MMP9-GFP fusion event traces (green channel) and time aligned to the red channel. Background-subtracted and normalized fluorescence intensity traces are shown for each protein.

Supplemental Figure 2: Average time-lapse traces of normalized fluorescence intensities signal (dark line) of red fluorescent-labeled (A) PA-sensor, *N*=3; (B) DGKA, *N*=6; (C) DGKD, *N*=3; (D) DGKG, *N*=4 and the SE of the data in (gray) for all traces. Dashed line marks the zero-time point that was generated from individual MMP9-GFP fusion event traces (green channel) and time aligned to the red channel. Background-subtracted and normalized fluorescence intensity traces are shown for each protein.

Discussion

The process of regulated exocytosis has been a topic of research for several decades and has led to the discovery of a host of different proteins and lipids involved throughout this process. During exocytosis, the core machinery of the SNARE proteins, in the form of VAMPs, syntaxins, and SNAP proteins, are essential components of the exocytic molecular machinery facilitating fusion of secretory vesicles and release of cargo. Although there is much evidence suggesting that SNARE proteins play a key role in the fusion machinery, other cellular elements regulating exocytosis have received less attention. Among those factors, specialized lipids have also been proposed to have important functions during exocytosis, both at the level of secretory vesicle recruitment and late-stage membrane fusion steps. The regulatory lipid, PIP2, is the best example of the involvement of a lipid in regulated exocytosis, with roles in membrane fusion associated with regulated DCV exocytosis in neuroendocrine cells, synaptic vesicles exocytosis in neurons, and constitutive vesicle exocytosis in a variety of cell types [51]. There is growing evidence suggesting that PIP2 acts as a key organizing "element", enriched in microdomains of the plasma membrane, spatially defining the position of exocytic sites and temporally identifying the precise timing of membrane fusion events [24, 50, 51]. Such enrichment of PIP2 at exocytic sites in neuroendocrine cells was shown to recruit and activate the effector proteins (*i.e.* PIP2-binding proteins), CAPS and MUNC13, both of which function in vesicle priming to facilitate this organization of SNARE proteins [27, 98]. Overall, the regulatory lipid, PIP2, is functionally implicated in regulated exocytosis and suggests it, as well as other lipids, act as possible organizing "elements" identifying exocytic sites in cells. This spatial and temporal organization is presumably accomplished through the local synthesis and degradation of PIP2 at these spatiotemporally defined sites of membrane fusion.

Here, we investigated the spatiotemporal organization and dynamics of specialized lipids surrounding the PIP2-mediated signaling pathway at fusing secretory vesicles containing the pro-tumor marker, MMP-9 in living MCF-7 breast cancer cells. We used TIRF to probe the lipid environment, and effectors proteins associated with these lipids, at exocytic sites, in an attempt to better define their spatial patterning, and temporal dynamic behavior, during membrane fusion at exocytic sites of MMP-9. To this end, we systematically spatially mapped and determined the temporal dynamics of key specialized lipids and proteins, implicated in the PIP2-mediated signaling pathway, to individual exocytic sites of MMP-9 in MCF-7 cells. The major synthetic pathway for the formation of PIP2 (*i.e.* PIP2-mediated signaling pathway; Figure 9) utilized by cells, involves a cascade of lipids. These specialized lipids are spatially and temporally regulated through the actions of kinases, phosphatases, and phospholipase, which are locally synthesized or accumulated at exocytic sites of MMP-9 [24, 27, 45, 50-52]. Consistent with this idea, the dynamic behavior of several lipids observed using two-color TIRF revealed an accumulation of several lipids, (*e.g.* PIP, PIP2, and DAG), as well as, some lipid kinase isoforms responsible for their synthesis (*e.g.* PI4K2B, PI4K3A, and PIP5KA) and several downstream protein kinase isoform effectors (*e.g.* PRKCA and PRKCE) at exocytic sites of MMP-9 in MCF-7 cells. From our data, we identified one general dynamic behavior (*i.e.* transient accumulation around the time of membrane fusion) of lipid-sensors, lipid kinases, and protein kinases (red channel) at sites of exocytosis of MMP-9 (green channel). Spatial patterning and temporal dynamic measurements suggest that these molecules are not highly colocalized or enriched at docked secretory vesicles containing MMP-9 in the absence of PMA. However, following stimulation with PMA, which triggers regulated exocytosis, many of these molecules showed rapid and transient accumulation at exocytic sites. This accumulation centered around the moment of cargo release and was followed by a slow decay. We speculate that the rapid, yet transient accumulation of these specialized lipids (and effector proteins) at exocytic sites could represent the formation of microdomains that help facilitate exocytosis as has been previously suggested with the PIP2-mediated signaling pathway [24, 50, 51].

The PIP2-mediated signaling pathways begins with a series of sequential phosphorylations on PIs by several PI-specific lipid kinases, to generate first the lipid, PI4P (or PIP), followed by the regulatory lipid, PIP2. This sequential phosphorylation of PIs (major pathway) is accomplished by the lipid kinases, PI4K and PIP5K, respectively [74, 99]. After stimulation with PMA, we observed an enrichment of the lipid, PI4P, using the PIP^{P4M} lipid sensor (Figure 3A) and two isoforms of the PI-specific lipid kinase, PI4K, using, PI4K2B and PI4K3A (Figure 4B & 4C), at exocytic sites around the time of fusion and release of MMP-9. The next sequential step in PIP2 synthesis is the conversion of PI4P (or PIP) into PIP2 by the PI-specific kinase, PIP5K. We observed a rapid and transient accumulation of the regulatory lipid, PIP2 (Figure 2B) during exocytosis of MMP-9 and accumulation of the PIP5KG isoform (Figure 5C) prior to exocytosis of MMP-9. Collectively, this data points to an essential spatial and temporal role of the lipids and PI-specific lipid kinases at exocytic sites and the release of the secretory vesicle cargo, MMP-9. We hypothesize that the PI-derived lipids, PIP and PIP2 are locally synthesized at fusion sites during exocytosis of MMP-9. This accumulation of lipids at exocytic sites, spatially and temporally defines the position of the site and precise timing associated with fusion and cargo release. Moreover, the accumulation of PIP and PIP2 is accomplished through the local accumulation, at exocytic sites around the moment of fusion, of the lipid kinases isoforms, PI4K2B, PI4K3A, and PIP5KA, responsible for their synthesis. This increased concentration in PIP2 (*i.e.* PIP2-rich

membrane domains or PIP2 microdomains) at exocytic sites is consistent with recent evidence showing PIP2-rich regions localized to sites of vesicle exocytosis in neuroendocrine cells [27].

For the four PI4K variants tested (Figure 4A-D), PI4K2A isoform showed prolonged enrichment at fusion sites during and after exocytosis, while the PI4K2B isoform showed transient enrichment after exocytosis. However, the PI4K3A isoform showed a rapid yet transient accumulation centered on the moment of membrane fusion at exocytic sites, while the PI4K3B isoform showed no change in fluorescence signal before, during, or after membrane fusion events. While, using the PIP5K isoforms, we only see a transient accumulation of PIP5KA, and this buildup occurs immediately before exocytosis of MMP-9 (Figure 5A). Overall, taken together, we believe the live-cell imaging data of the various PI4K and PI5PK isoforms implies a distinct spatial and temporal organization at sites of exocytosis of MMP-9 in MCF-7 cells. Additionally, this data is consistent with known function and spatial patterning of the various PI-specific lipid kinase isoforms, as has been previously suggested [74, 100] and suggests their involvement at exocytic sites of MMP-9 in MCF-7 cells.

In the PIP2-mediated signaling pathway (Figure 9), PIP2 levels can be regulated by the PI-specific lipid kinases that lead to PIP2 synthesis. However, PIP2 concentrations can also be regulated by the degradation of PIP2 by PLC, into DAG, which acts as a secondary messenger to activate the downstream effectors: (1) lipid kinase family, DGKs; or (2), protein kinase family, PRKCs. We observed evidence of PIP2 degradation to DAG at exocytic sites, through the use of the DAG-specific lipid sensor. We observed a transient accumulation of DAG (Figure 2D), during exocytosis of MMP-9, with kinetics broadly similar to that observed with PIP2. As it relates to DGK, a downstream effector of DAG, we did not observe any fluorescence dynamic changes associated with DGK isoforms or with the PA-lipid sensor, following DGK activity on DAG (Supplemental Figure 2). As it relates to PRKC, the other downstream effector of DAG, we observed a rapid, yet transient accumulation of several of the PRKC isoforms (PRKCA and PRKCE), during the exact moment of fusion, at exocytic sites of MMP-9 (Figure 6A & 6E). This is similar to that detected for the DAG lipid sensor and again suggests possible isoform specific spatial and temporal roles of the various PRKCs at exocytic sites during membrane fusion. We hypothesize that DAG acts at sites of exocytosis of MMP-9, to possibly recruit and activate PRKCs to potentially phosphorylate exocytic proteins at fusion sites. Consistent with this view, PRKCs have been linked to the regulated exocytosis of insulin in neuroendocrine cells and presumably targets several different exocytic proteins [43, 101, 102].

In neuroendocrine, PC12 cells, PRKC phosphorylates several exocytic proteins, including munc18, SNAP25, and synaptotagmin [83, 86, 103, 104], and this phosphorylation facilitates regulated exocytosis in these cells by modulating membrane-attached exocytic machinery [105]. We hypothesize that a similar scenario exists in MCF-7 cells, where PRKC is locally recruited to exocytic sites, during the moment of membrane fusion. This would allow the PRKCs to phosphorylate a variety of proteins associated with fusogenic secretory vesicles containing MMP-9. We are currently trying to identify potential targets of phosphorylation, in response to the recruitment of PRKC that we observed at exocytic sites. Identification of targets of phosphorylation by PRKC, in non-neuronal cells, like MCF-7 cells, has proven to be rather difficult due to the unavailability of phospho-specific antibodies used to detect phosphorylated target proteins, as compared to those available for the same family of proteins in neuronal cells, like PC12 cells. Although, we are not able to report multiple targets of phosphorylation by PRKC, our blots suggest that Rabphilin, a Rab effector protein, is a potential target (Figure 7). Moreover, we showed using super-resolution TIRF-SIM that after stimulation with PMA, there is close

proximity (*i.e.* colocalization) between PRKCE and secretory vesicles containing MMP-9 (Figure 7). Overall, our data showed isoform-specific PRKC locally accumulated at exocytic sites of MMP-9 and suggests a possible spatial and temporal role of PRKC at exocytic sites in MCF-7 cells.

Our TIRF-based imaging data show that the PIP2-mediated signaling pathway is involved in the spatiotemporal organization during membrane fusion, at exocytic sites of MMP-9 in MCF-7 cells. More importantly this cascade of lipids in the pathway may serve as organizing "elements", spatially and temporally coordinating regulated exocytosis in these breast cancer cells. We systematically mapped out the dynamic behavior of the lipid signaling cascade from PI to PRKC. The lipids, which include PIP, PIP2, and DAG, are regulated at the level of synthesis and degradation, through the interconversion by specific kinases and phospholipases, that locally control the concentrations of these lipids at sites of exocytosis. Our results showed that the lipids in the PIP2 signaling pathway are locally synthesized or recruited to exocytic sites of MMP-9 in MCF-7 cells, at precisely the moment of fusion, and their transient accumulation is also accompanied by transient accumulation of the enzymes involved in their synthesis or their downstream effectors, including lipid kinases and protein kinases (*i.e.* PRKCs), respectively. The low spatial patterning or low colocalization, as well as, the temporal dynamic behavior (*i.e.* rapid, yet transient accumulation) associated with the specialized lipids (*i.e.* organizing "element" #2) at exocytic sites contrasts drastically with the high colocalization and decisively different temporal dynamics associated with the specialized scaffolding proteins (organizing "element" #1), like the Rab proteins (*e.g.* Rab27a and Rab27b, Figure 8), Rab effector proteins (*e.g.* Rabphilin and hSlp-4), and SNARE proteins (*e.g.* VAMP3) at these same exocytic sites in MCF-7 cells [58]. We found that many regulators of exocytosis, including several Rab GTPases, Rab effector proteins, and SNARE/SNARE modulator proteins, are stably assembled on docked secretory vesicles before exocytosis. At the moment of fusion, many of these components are slowly lost from the vesicle via lateral diffusion to the plasma membrane [58]. The rapid yet transient accumulation of several specialized lipids or organizing "element" #2 that we observed at sites of exocytosis, during the moment of membrane fusion, is to our knowledge the first systematic examination of the dynamic temporal behavior of lipids surrounding the PIP2-mediated signaling pathway.

Additionally, our results reiterate the utility and broad applicability of this two-color TIRF imaging-based approach for systematically mapping the molecular composition, spatial organization, and dynamic temporal behavior of discrete cellular processes like that surrounding regulated exocytosis [56-58, 67]. It is important to note that all of the spatiotemporal information we acquired using this TIRF method implies only correlative associations. Specifically, the recruitment of lipid sensors and tagged kinase enzymes (*i.e.* lipid kinases and protein kinases) involved in PIP2-mediated signaling pathway to exocytic sites is correlated with the exocytosis of MMP-9 from secretory vesicles in MCF-7 cells and does not prove a functional or mechanistic connection with exocytosis. The goal of this imaging-based TIRF method was to establish the spatial organization and temporal dynamics of specialized lipids (organizing element #2) associated with membrane fusion, at exocytic sites of MMP-9 in MCF-7 cells. This work is meant to complement, not replace, traditional functional studies used to probe the spatiotemporal organization associated with these exocytic sites. Future biochemistry studies will be essential in directly uncovering the functional associations of these specialized lipids (organizing element #2) at sites of regulated exocytosis of the pro-tumor marker, MMP-9 in MCF-7 breast cancer cells and could further our understanding of cancer progression and metastasis.

Conclusions

Our current understanding of the spatial organization and temporal dynamics associated with the three distinct categories of organizing "elements" (i.e. scaffolding proteins, specialized lipids, and the actin cytoskeleton network) during regulated exocytosis has come extensively from a limited number of categories of secretory cell types. There are four major categories of cells capable of undergoing regulated exocytosis, including neuronal, endocrine, exocrine, and hematopeoietic cells [106]. However, an overwhelming majority of the information known about regulated exocytosis comes from either neuronal or endocrine cells types, using a limited number of secretory vesicle markers specific to those cell types. Therefore, the discovery that MMP9-GFP could be used to image regulated exocytosis in the exocrine, MCF-7 cells line, allows us to understand the spatial organization and temporal dynamics associated with protein and lipid involvement in regulated exocytosis in other secretory cell types [58]. We used the TIRF-based imaging system to systematically determine the spatial organization and temporal dynamics of lipids (and effector proteins) associated with membrane fusion and exocytosis of MMP-9 in MCF-7 cells. The local accumulation of the PIP2-mediated signaling lipids, like PIP, PIP2, and DAG at exocytic sites of MMP-9, during PMA-stimulated exocytosis in MCF-7 cells, establishes local enrichment or accumulation of these specialized lipids to exocytic sites. These specialized lipids can facilitate possible protein-lipid interactions needed at exocytic sites and provide possible protein-recruiting mechanisms that offer additional supplementary levels of control of the exocytic machinery in the cell. These lipid factors, to some extent, directly regulate the release of vesicle cargo and future studies will be necessary to discover how these lipids and their known protein effectors control regulated exocytosis, via spatiotemporal organization, in a variety of secretory cell types, using different secretory vesicle markers.

Abbreviations

MMP-9, matrix metalloproteinase-9; SNAREs, soluble N-ethylmaleimide–sensitive factor attachment protein receptors; PIP, phosphatidylinositol 4-phosphate; PIP2, phosphatidylinositol-4,5-biphosphate; DAG, diacylglycerol; DGK, diacylglycerol kinase; PMA, phorbol myristate acetate; PI4K, phosphatidylinositol 4-kinase; PIP5K, phosphatidylinositol 4-phosphate 5-kinase; PRKC, protein kinase C.

Declarations

Ethics approval and consent to participate: Not applicable.

Consent for publication: Not applicable.

Availability of data and materials: The datasets used and/or analyzed during the current study are available form the corresponding author on reasonable request.

Competing interests: No competing interests.

Funding: D.A. Harris is supported by the National Science Foundation (#1891204). J.W. Taraska is supported by the Intramural Research Program of the National Heart, Lung, and Blood Institute, National Institutes of Health.

Author contributions and Acknowledgements: D.A. Harris and J.W. Taraska designed the study, D.C. Stephens and D.A. Harris performed experiments, and D.C. Stephens and D.A. Harris analyzed data and wrote the manuscript.

Acknowledgements: D.A. Harris is supported by the National Science Foundation (#1891204). J.W. Taraska is supported by the Intramural Research Program of the National Heart, Lung, and Blood Institute, National Institutes of Health.

References

1. Mostov, K.E., M. Verges, and Y. Altschuler, *Membrane traffic in polarized epithelial cells.* Curr Opin Cell Biol, 2000. **12**(4): p. 483-90.
2. Winkle, C.C., et al., *A novel Netrin-1-sensitive mechanism promotes local SNARE-mediated exocytosis during axon branching.* J Cell Biol, 2014. **205**(2): p. 217-32.
3. Harris, D.A., et al., *Exosomes released from breast cancer carcinomas stimulate cell movement.* PLoS One, 2015. **10**(3): p. e0117495.
4. Hendrix, A., et al., *An ex(o)citing machinery for invasive tumor growth.* Cancer Res, 2010. **70**(23): p. 9533-7.
5. Wan, Z., et al., *Exosome-mediated cell-cell communication in tumor progression.* Am J Cancer Res, 2018. **8**(9): p. 1661-1673.
6. Gucek, A., et al., *Fusion pore regulation by cAMP/Epac2 controls cargo release during insulin exocytosis.* Elife, 2019. **8**.
7. Lu, P., et al., *Extracellular matrix degradation and remodeling in development and disease.* Cold Spring Harb Perspect Biol, 2011. **3**(12).
8. Weigelt, B., J.L. Peterse, and L.J. van 't Veer, *Breast cancer metastasis: markers and models.* Nat Rev Cancer, 2005. **5**(8): p. 591-602.
9. Singh, D., et al., *Multifaceted role of matrix metalloproteinases (MMPs).* Front Mol Biosci, 2015. **2**: p. 19.
10. Stetler-Stevenson, W.G., *The role of matrix metalloproteinases in tumor invasion, metastasis, and angiogenesis.* Surg Oncol Clin N Am, 2001. **10**(2): p. 383-92, x.
11. Stetler-Stevenson, W.G. and A.E. Yu, *Proteases in invasion: matrix metalloproteinases.* Semin Cancer Biol, 2001. **11**(2): p. 143-52.
12. Mendes, O., H.T. Kim, and G. Stoica, *Expression of MMP2, MMP9 and MMP3 in breast cancer brain metastasis in a rat model.* Clin Exp Metastasis, 2005. **22**(3): p. 237-46.
13. Saito, T., et al., *Overexpressed progesterone receptor form B inhibit invasive activity suppressing matrix metalloproteinases in endometrial carcinoma cells.* Cancer Lett, 2004. **209**(2): p. 237-43.
14. Seftor, R.E., et al., *Cooperative interactions of laminin 5 gamma2 chain, matrix metalloproteinase-2, and membrane type-1-matrix/metalloproteinase are required for mimicry of embryonic vasculogenesis by aggressive melanoma.* Cancer Res, 2001. **61**(17): p. 6322-7.
15. Zhang, B., et al., *Matrix metalloproteinase-2 (MMP-2) expression and regulation by tumor necrosis factor alpha (TNFalpha) in the bovine corpus luteum.* Mol Reprod Dev, 2005. **70**(2): p. 122-32.

16. Cao, J., et al., *Membrane type 1-matrix metalloproteinase promotes human prostate cancer invasion and metastasis.* Thromb Haemost, 2005. **93**(4): p. 770-8.
17. Schnaeker, E.M., et al., *Microtubule-dependent matrix metalloproteinase-2/matrix metalloproteinase-9 exocytosis: prerequisite in human melanoma cell invasion.* Cancer Res, 2004. **64**(24): p. 8924-31.
18. Jahn, R. and D. Fasshauer, *Molecular machines governing exocytosis of synaptic vesicles.* Nature, 2012. **490**(7419): p. 201-7.
19. Sudhof, T.C., *The synaptic vesicle cycle.* Annu Rev Neurosci, 2004. **27**: p. 509-47.
20. Sollner, T., et al., *A protein assembly-disassembly pathway in vitro that may correspond to sequential steps of synaptic vesicle docking, activation, and fusion.* Cell, 1993. **75**(3): p. 409-18.
21. Sollner, T., et al., *SNAP receptors implicated in vesicle targeting and fusion.* Nature, 1993. **362**(6418): p. 318-24.
22. Kean, M.J., et al., *VAMP3, syntaxin-13 and SNAP23 are involved in secretion of matrix metalloproteinases, degradation of the extracellular matrix and cell invasion.* J Cell Sci, 2009. **122**(Pt 22): p. 4089-98.
23. Sudhof, T.C. and J.E. Rothman, *Membrane fusion: grappling with SNARE and SM proteins.* Science, 2009. **323**(5913): p. 474-7.
24. Gundelfinger, E.D., M.M. Kessels, and B. Qualmann, *Temporal and spatial coordination of exocytosis and endocytosis.* Nat Rev Mol Cell Biol, 2003. **4**(2): p. 127-39.
25. Balla, T., *Phosphoinositides: tiny lipids with giant impact on cell regulation.* Physiol Rev, 2013. **93**(3): p. 1019-137.
26. Cremona, O. and P. De Camilli, *Phosphoinositides in membrane traffic at the synapse.* J Cell Sci, 2001. **114**(Pt 6): p. 1041-52.
27. Kabachinski, G., et al., *CAPS and Munc13 utilize distinct PIP2-linked mechanisms to promote vesicle exocytosis.* Mol Biol Cell, 2014. **25**(4): p. 508-21.
28. Martin, T.F., *PI(4,5)P(2)-binding effector proteins for vesicle exocytosis.* Biochim Biophys Acta, 2015. **1851**(6): p. 785-93.
29. Zhang, L., et al., *Phosphatidylinositol 4, 5 bisphosphate and the actin cytoskeleton.* Subcell Biochem, 2012. **59**: p. 177-215.
30. Zhang, X., X. Li, and H. Xu, *Phosphoinositide isoforms determine compartment-specific ion channel activity.* Proc Natl Acad Sci U S A, 2012. **109**(28): p. 11384-9.
31. Eberhard, D.A., et al., *Evidence that the inositol phospholipids are necessary for exocytosis. Loss of inositol phospholipids and inhibition of secretion in permeabilized cells caused by a bacterial phospholipase C and removal of ATP.* Biochem J, 1990. **268**(1): p. 15-25.
32. Wen, P.J., et al., *Phosphatidylinositol(4,5)bisphosphate coordinates actin-mediated mobilization and translocation of secretory vesicles to the plasma membrane of chromaffin cells.* Nat Commun, 2011. **2**: p. 491.
33. James, D.J., et al., *Phosphatidylinositol 4,5-bisphosphate regulates SNARE-dependent membrane fusion.* J Cell Biol, 2008. **182**(2): p. 355-66.
34. Smindak, R.J., et al., *Lipid-dependent regulation of exocytosis in S. cerevisiae by OSBP homolog (Osh) 4.* J Cell Sci, 2017. **130**(22): p. 3891-3906.
35. Bauer, C.S., et al., *Potentiation of exocytosis by phospholipase C-coupled G-protein-coupled receptors requires the priming protein Munc13-1.* J Neurosci, 2007. **27**(1): p. 212-9.
36. Manifava, M., et al., *Differential binding of traffic-related proteins to phosphatidic acid- or phosphatidylinositol (4,5)- bisphosphate-coupled affinity reagents.* J Biol Chem, 2001. **276**(12): p. 8987-94.
37. Nakanishi, H., P. de los Santos, and A.M. Neiman, *Positive and negative regulation of a SNARE protein by control of intracellular localization.* Mol Biol Cell, 2004. **15**(4): p. 1802-15.

38. Rizzo, M. and G. Romero, *Pharmacological importance of phospholipase D and phosphatidic acid in the regulation of the mitogen-activated protein kinase cascade.* Pharmacol Ther, 2002. **94**(1-2): p. 35-50.
39. Barclay, J.W., et al., *Phosphorylation of Munc18 by protein kinase C regulates the kinetics of exocytosis.* J Biol Chem, 2003. **278**(12): p. 10538-45.
40. Pozzi, D., et al., *Activity-dependent phosphorylation of Ser187 is required for SNAP-25-negative modulation of neuronal voltage-gated calcium channels.* Proc Natl Acad Sci U S A, 2008. **105**(1): p. 323-8.
41. Rickman, C. and R.R. Duncan, *Munc18/Syntaxin interaction kinetics control secretory vesicle dynamics.* J Biol Chem, 2010. **285**(6): p. 3965-72.
42. Yang, Y., et al., *Phosphomimetic mutation of Ser-187 of SNAP-25 increases both syntaxin binding and highly Ca2+-sensitive exocytosis.* J Gen Physiol, 2007. **129**(3): p. 233-44.
43. Morgan, A., et al., *Regulation of exocytosis by protein kinase C.* Biochem Soc Trans, 2005. **33**(Pt 6): p. 1341-4.
44. de Jong, A.P., et al., *Phosphorylation of synaptotagmin-1 controls a post-priming step in PKC-dependent presynaptic plasticity.* Proc Natl Acad Sci U S A, 2016. **113**(18): p. 5095-100.
45. Ammar, M.R., et al., *Lipids in Regulated Exocytosis: What are They Doing?* Front Endocrinol (Lausanne), 2013. **4**: p. 125.
46. Antal, C.E. and A.C. Newton, *Spatiotemporal dynamics of phosphorylation in lipid second messenger signaling.* Mol Cell Proteomics, 2013. **12**(12): p. 3498-508.
47. Barylko, B., et al., *A novel family of phosphatidylinositol 4-kinases conserved from yeast to humans.* J Biol Chem, 2001. **276**(11): p. 7705-8.
48. Gromada, J., et al., *Neuronal calcium sensor-1 potentiates glucose-dependent exocytosis in pancreatic beta cells through activation of phosphatidylinositol 4-kinase beta.* Proc Natl Acad Sci U S A, 2005. **102**(29): p. 10303-8.
49. Wiedemann, C., T. Schafer, and M.M. Burger, *Chromaffin granule-associated phosphatidylinositol 4-kinase activity is required for stimulated secretion.* EMBO J, 1996. **15**(9): p. 2094-101.
50. Hilgemann, D., *Local PIP2 signals: When, where, and how?* Pflügers Archiv : European journal of physiology, 2007. **455**: p. 55-67.
51. Martin, T.F., *Role of PI(4,5)P(2) in vesicle exocytosis and membrane fusion.* Subcell Biochem, 2012. **59**: p. 111-30.
52. Chasserot-Golaz, S., et al., *Lipid dynamics in exocytosis.* Cell Mol Neurobiol, 2010. **30**(8): p. 1335-42.
53. Urbina, F.L., S.M. Gomez, and S.L. Gupton, *Spatiotemporal organization of exocytosis emerges during neuronal shape change.* J Cell Biol, 2018. **217**(3): p. 1113-1128.
54. Yuan, T., et al., *Spatiotemporal detection and analysis of exocytosis reveal fusion "hotspots" organized by the cytoskeleton in endocrine cells.* Biophys J, 2015. **108**(2): p. 251-60.
55. Hogue, I.B., J. Scherer, and L.W. Enquist, *Exocytosis of Alphaherpesvirus Virions, Light Particles, and Glycoproteins Uses Constitutive Secretory Mechanisms.* mBio, 2016. **7**(3).
56. Somasundaram, A. and J.W. Taraska, *Local protein dynamics during microvesicle exocytosis in neuroendocrine cells.* Mol Biol Cell, 2018. **29**(15): p. 1891-1903.
57. Trexler, A.J., K.A. Sochacki, and J.W. Taraska, *Imaging the recruitment and loss of proteins and lipids at single sites of calcium-triggered exocytosis.* Mol Biol Cell, 2016. **27**(15): p. 2423-34.
58. Stephens, D., et al., *Spatiotemporal organization and protein dynamics involved in regulated exocytosis of MMP-9 in breast cancer cells.* J Gen Physiol, 2019. **In press**.

59. Holz, R.W., et al., *A pleckstrin homology domain specific for phosphatidylinositol 4, 5-bisphosphate (PtdIns-4,5-P2) and fused to green fluorescent protein identifies plasma membrane PtdIns-4,5-P2 as being important in exocytosis.* J Biol Chem, 2000. **275**(23): p. 17878-85.
60. Maekawa, M. and G.D. Fairn, *Molecular probes to visualize the location, organization and dynamics of lipids.* J Cell Sci, 2014. **127**(Pt 22): p. 4801-12.
61. Platre, M.P. and Y. Jaillais, *Guidelines for the Use of Protein Domains in Acidic Phospholipid Imaging.* Methods Mol Biol, 2016. **1376**: p. 175-94.
62. Codazzi, F., M.N. Teruel, and T. Meyer, *Control of astrocyte Ca(2+) oscillations and waves by oscillating translocation and activation of protein kinase C.* Curr Biol, 2001. **11**(14): p. 1089-97.
63. Stauffer, T.P., S. Ahn, and T. Meyer, *Receptor-induced transient reduction in plasma membrane PtdIns(4,5)P2 concentration monitored in living cells.* Curr Biol, 1998. **8**(6): p. 343-6.
64. Hammond, G.R., M.P. Machner, and T. Balla, *A novel probe for phosphatidylinositol 4-phosphate reveals multiple pools beyond the Golgi.* J Cell Biol, 2014. **205**(1): p. 113-26.
65. Johannessen, C.M., et al., *COT drives resistance to RAF inhibition through MAP kinase pathway reactivation.* Nature, 2010. **468**(7326): p. 968-72.
66. Antonescu, C.N., et al., *Phosphatidylinositol-(4,5)-bisphosphate regulates clathrin-coated pit initiation, stabilization, and size.* Mol Biol Cell, 2011. **22**(14): p. 2588-600.
67. Larson, B.T., et al., *Systematic spatial mapping of proteins at exocytic and endocytic structures.* Mol Biol Cell, 2014. **25**(13): p. 2084-93.
68. Ran, F.A., et al., *Double nicking by RNA-guided CRISPR Cas9 for enhanced genome editing specificity.* Cell, 2013. **154**(6): p. 1380-9.
69. Ran, F.A., et al., *Genome engineering using the CRISPR-Cas9 system.* Nat Protoc, 2013. **8**(11): p. 2281-2308.
70. Masur, S.K., V. Sapirstein, and D. Rivero, *Phorbol myristate acetate induces endocytosis as well as exocytosis and hydroosmosis in toad urinary bladder.* Biochim Biophys Acta, 1985. **821**(2): p. 286-96.
71. Aikawa, Y. and T.F. Martin, *ARF6 regulates a plasma membrane pool of phosphatidylinositol(4,5)bisphosphate required for regulated exocytosis.* J Cell Biol, 2003. **162**(4): p. 647-59.
72. Trexler, A.J. and J.W. Taraska, *Regulation of insulin exocytosis by calcium-dependent protein kinase C in beta cells.* Cell Calcium, 2017. **67**: p. 1-10.
73. Xue, R., Y. Zhao, and P. Chen, *Involvement of PKC alpha in PMA-induced facilitation of exocytosis and vesicle fusion in PC12 cells.* Biochem Biophys Res Commun, 2009. **380**(2): p. 371-6.
74. van den Bout, I. and N. Divecha, *PIP5K-driven PtdIns(4,5)P2 synthesis: regulation and cellular functions.* J Cell Sci, 2009. **122**(Pt 21): p. 3837-50.
75. Roy, A. and T.P. Levine, *Multiple pools of phosphatidylinositol 4-phosphate detected using the pleckstrin homology domain of Osh2p.* J Biol Chem, 2004. **279**(43): p. 44683-9.
76. Stefan, C.J., et al., *Osh proteins regulate phosphoinositide metabolism at ER-plasma membrane contact sites.* Cell, 2011. **144**(3): p. 389-401.
77. Hay, J.C., et al., *ATP-dependent inositide phosphorylation required for Ca(2+)-activated secretion.* Nature, 1995. **374**(6518): p. 173-7.
78. Gillis, K.D., R. Mossner, and E. Neher, *Protein kinase C enhances exocytosis from chromaffin cells by increasing the size of the readily releasable pool of secretory granules.* Neuron, 1996. **16**(6): p. 1209-20.
79. Pocotte, S.L., et al., *Effects of phorbol ester on catecholamine secretion and protein phosphorylation in adrenal medullary cell cultures.* Proc Natl Acad Sci U S A, 1985. **82**(3): p. 930-4.

80. Shoji-Kasai, Y., et al., *Protein kinase C-mediated translocation of secretory vesicles to plasma membrane and enhancement of neurotransmitter release from PC12 cells.* Eur J Neurosci, 2002. **15**(8): p. 1390-4.
81. Vitale, M.L., E.P. Seward, and J.M. Trifaro, *Chromaffin cell cortical actin network dynamics control the size of the release-ready vesicle pool and the initial rate of exocytosis.* Neuron, 1995. **14**(2): p. 353-63.
82. Nagy, G., et al., *Protein kinase C-dependent phosphorylation of synaptosome-associated protein of 25 kDa at Ser187 potentiates vesicle recruitment.* J Neurosci, 2002. **22**(21): p. 9278-86.
83. Shimazaki, Y., et al., *Phosphorylation of 25-kDa synaptosome-associated protein. Possible involvement in protein kinase C-mediated regulation of neurotransmitter release.* J Biol Chem, 1996. **271**(24): p. 14548-53.
84. Haberman, Y., et al., *Classical protein kinase C(s) regulates targeting of synaptotagmin IX to the endocytic recycling compartment.* J Cell Sci, 2005. **118**(Pt 8): p. 1641-9.
85. Roggero, C.M., et al., *Protein kinase C-mediated phosphorylation of the two polybasic regions of synaptotagmin VI regulates their function in acrosomal exocytosis.* Dev Biol, 2005. **285**(2): p. 422-35.
86. Fujita, Y., et al., *Phosphorylation of Munc-18/n-Sec1/rbSec1 by protein kinase C: its implication in regulating the interaction of Munc-18/n-Sec1/rbSec1 with syntaxin.* J Biol Chem, 1996. **271**(13): p. 7265-8.
87. Foletti, D.L., J.T. Blitzer, and R.H. Scheller, *Physiological modulation of rabphilin phosphorylation.* J Neurosci, 2001. **21**(15): p. 5473-83.
88. Tzeng, H.T., et al., *Phosphorylation of Rab37 by protein kinase C alpha inhibits the exocytosis function and metastasis suppression activity of Rab37.* Oncotarget, 2017. **8**(65): p. 108556-108570.
89. Hepp, R., et al., *Phosphorylation of SNAP-23 regulates exocytosis from mast cells.* J Biol Chem, 2005. **280**(8): p. 6610-20.
90. Fitzgerald, M.L. and G.L. Reed, *Rab6 is phosphorylated in thrombin-activated platelets by a protein kinase C-dependent mechanism: effects on GTP/GDP binding and cellular distribution.* Biochem J, 1999. **342 (Pt 2)**: p. 353-60.
91. Ong, S.T., et al., *Phosphorylation of Rab5a protein by protein kinase C is crucial for T-cell migration.* J Biol Chem, 2014. **289**(28): p. 19420-34.
92. Pavarotti, M., et al., *Rab11 is phosphorylated by classical and novel protein kinase C isoenzymes upon sustained phorbol ester activation.* Biol Cell, 2012. **104**(2): p. 102-15.
93. Beach, J.R., et al., *Nonmuscle Myosin II Isoforms Coassemble in Living Cells.* Curr Biol, 2015. **25**(3): p. 402.
94. Brunstein, M., et al., *Full-field dual-color 100-nm super-resolution imaging reveals organization and dynamics of mitochondrial and ER networks.* Opt Express, 2013. **21**(22): p. 26162-73.
95. Guo, M., et al., *Single-shot super-resolution total internal reflection fluorescence microscopy.* Nat Methods, 2018. **15**(6): p. 425-428.
96. Pereira-Leal, J.B., A.N. Hume, and M.C. Seabra, *Prenylation of Rab GTPases: molecular mechanisms and involvement in genetic disease.* FEBS Lett, 2001. **498**(2-3): p. 197-200.
97. Novelli, G. and M.R. D'Apice, *Protein farnesylation and disease.* J Inherit Metab Dis, 2012. **35**(5): p. 917-26.
98. Grishanin, R.N., et al., *CAPS acts at a prefusion step in dense-core vesicle exocytosis as a PIP2 binding protein.* Neuron, 2004. **43**(4): p. 551-62.
99. Abel, K., R.A. Anderson, and S.B. Shears, *Phosphatidylinositol and inositol phosphate metabolism.* J Cell Sci, 2001. **114**(Pt 12): p. 2207-8.

100. Wong, K., R. Meyers dd, and L.C. Cantley, *Subcellular locations of phosphatidylinositol 4-kinase isoforms.* J Biol Chem, 1997. **272**(20): p. 13236-41.
101. Malaisse, W.J., et al., *Insulinotropic effect of the tumor promoter 12-O-tetradecanoylphorbol-13-acetate in rat pancreatic islets.* Cancer Res, 1980. **40**(10): p. 3827-31.
102. Virji, M.A., M.W. Steffes, and R.D. Estensen, *Phorbol myristate acetate: effect of a tumor promoter on insulin release from isolated rat islets of Langerhans.* Endocrinology, 1978. **102**(3): p. 706-11.
103. Hilfiker, S., et al., *Regulation of synaptotagmin I phosphorylation by multiple protein kinases.* J Neurochem, 1999. **73**(3): p. 921-32.
104. Slepnev, V.I., et al., *Role of phosphorylation in regulation of the assembly of endocytic coat complexes.* Science, 1998. **281**(5378): p. 821-4.
105. Chen, Y.A., et al., *Calmodulin and protein kinase C increase Ca(2+)-stimulated secretion by modulating membrane-attached exocytic machinery.* J Biol Chem, 1999. **274**(37): p. 26469-76.
106. Burgoyne, R.D. and M.J. Clague, *Calcium and calmodulin in membrane fusion.* Biochim Biophys Acta, 2003. **1641**(2-3): p. 137-43.

Figures

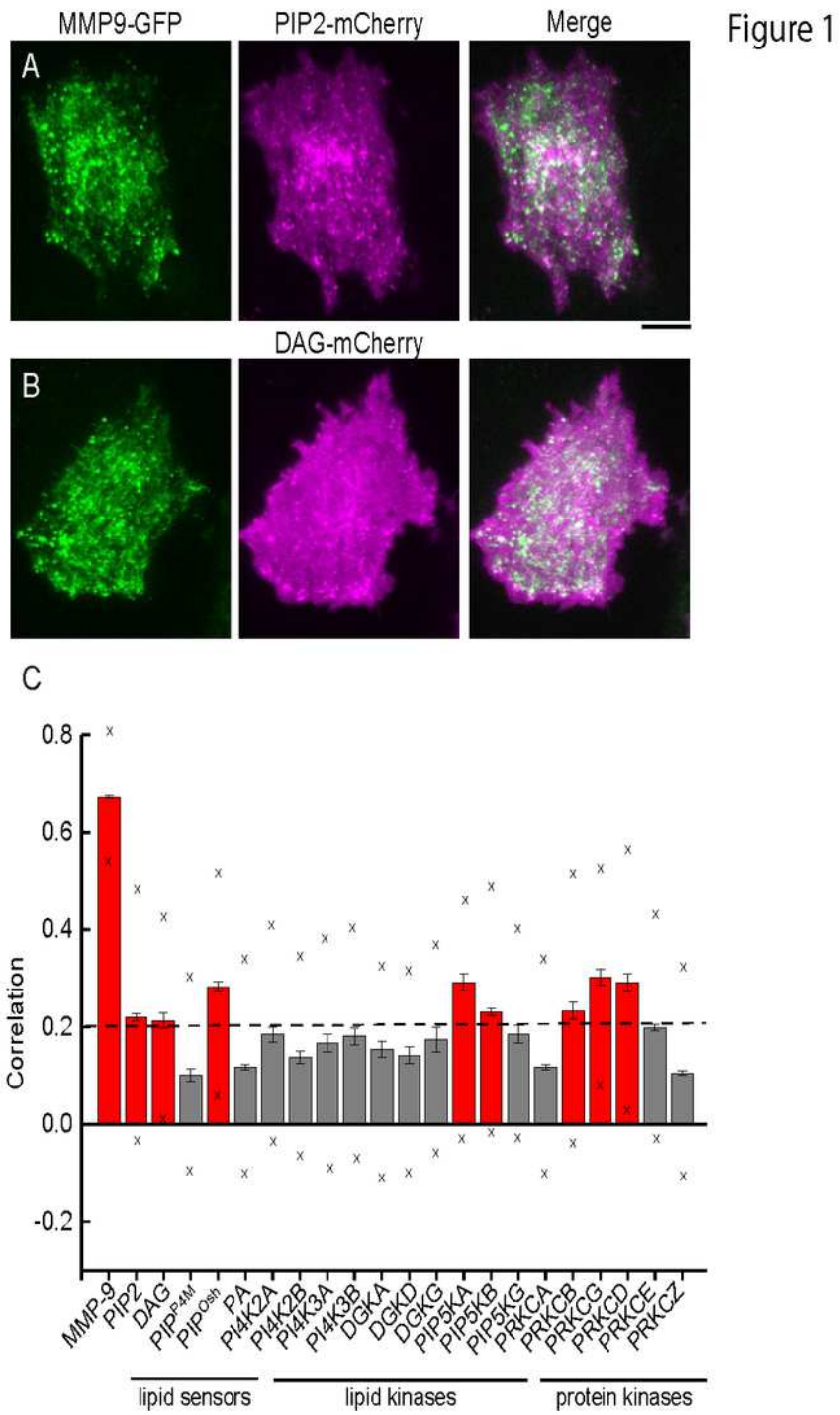

Figure 1

Figure 1

Representative TIRF images from the correlation analysis using lipid sensors tagged with a red-fluorescent protein associated with secretory vesicles, including images of MMP9-GFP, cotransfected with the: (A) PIP2-sensor; or (B) DAG-sensor. TIRF images from green channel of MMP9-GFP (left); red channel

of either PIP2-mCherry or DAG-mCherry lipid sensor (middle); and merge from both green and red channel (right) from a MCF-7 cell. Scale bar, 10μm. Correlation analysis with MMP9-GFP measures colocalization with secretory vesicles in uninduced cells. Shown is the correlation analysis of 22 proteins, which include lipid sensors, lipid kinase isoforms, and protein kinase C isoforms (PRKCs) with MMP9-GFP–labeled secretory vesicles in MCF-7 cells (C). Cells are sorted based on their position in the lipid signaling cascade. Red boxes above 0.2 (referenced by the dotted line) indicate proteins associated with secretory vesicles, and boxes below 0.2 indicate proteins that are nonspecifically or not associated with secretory vesicles. The whiskers are the standard error (SE) and the × marks above and below each data set are the standard deviation (SD). For all correlation assays using two-color TIRF, 15 cells were imaged from cotransfections with the MMP-GFP and a red fluorescently labeled protein.

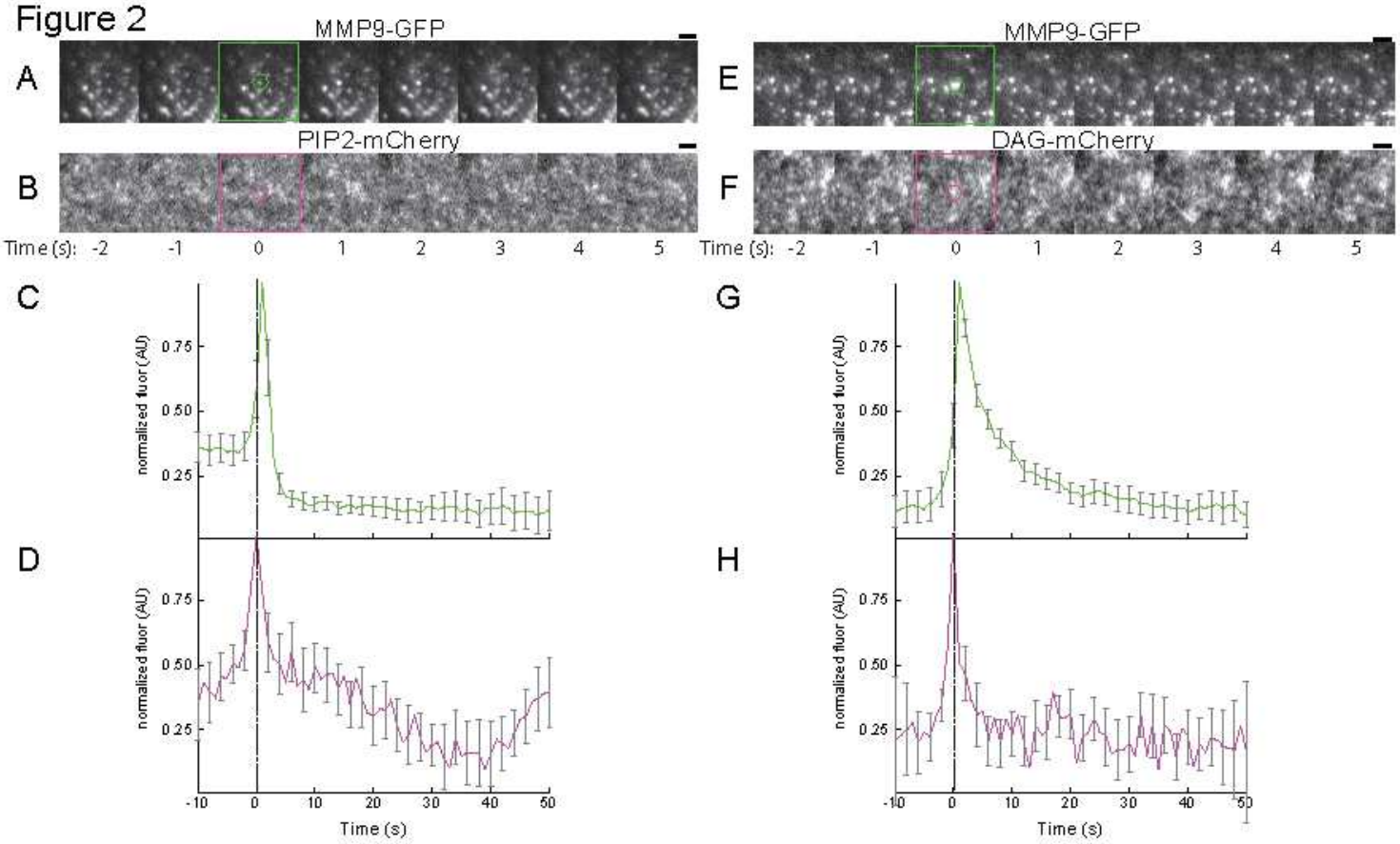

Figure 2: Gallery of representative TIRF images of MCF-7 cells transfected with MMP9-GFP and red fluorescent-labeled PIP2-sensor (A-D) and DAG-sensor (E-H). Shown is a fusion event in the green channel (A, E) and the corresponding region in the red channel for the PIP2-sensor (B) or DAG-sensor (F), following stimulation with PMA. Snapshots of the fusion event are at the indicated time-points. '0 s' is the manually identified first frame of brightening in the green channel. Circles (~1 μm diameter) represent regions used for intensity analysis. Average time-lapse traces of normalized fluorescence intensities for fusion events shown in the green (C & G) and red channels (D & H). Standard errors are plotted as (gray) areas around the average (green or red) trace. *N*=25 for PIP2 and 33 for DAG2. Dashed line marks the zero-time point that was generated from individual MMP9-GFP fusion event traces (green channel) and time aligned to the red channel. For all exocytosis assays using two-color TIRF, 15 cells were imaged from cotransfections with the MMP-GFP and a red fluorescently-labeled protein. A single coverslip with cells cotransfected with MMP9-GFP and a red-labeled protein were imaged.

Figure 2

Figure 3

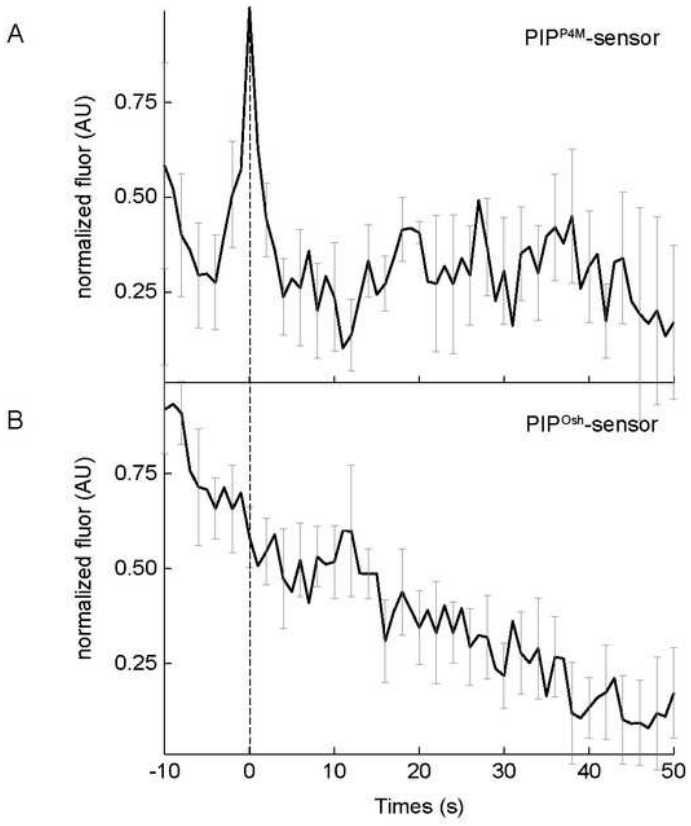

Figure 3: Average time-lapse traces of normalized fluorescence intensities signal (dark line) of the red fluorescent-labeled PI4P- or PIP-sensors, including: (A) PIP^{P4M}, *N*=15; and (B) PIP^{Osh}, *N*=19 and the SE of the data is show in (gray) for all traces. Dashed line marks the zero-time point that was generated from individual MMP9-GFP fusion event traces (green channel) and time aligned to the red channel. Background-subtracted and normalized fluorescence intensity traces are shown for each protein.

Figure 3

Figure 4

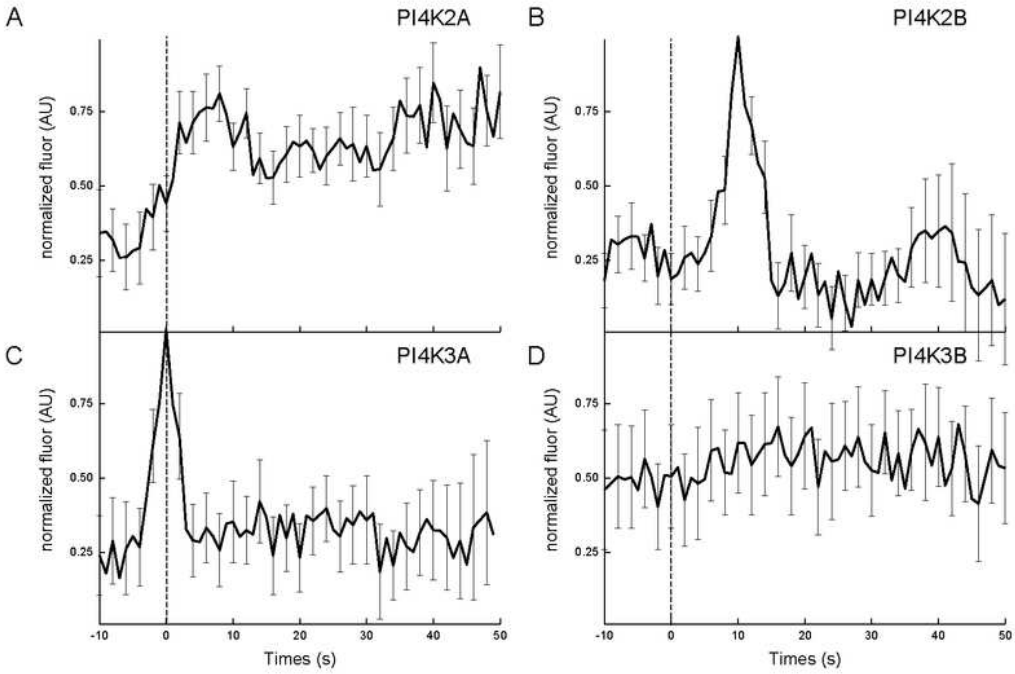

Figure 4: Average time-lapse traces of normalized fluorescence intensities signal (dark line) of red fluorescent-labeled lipid kinase isoforms, including: (A) PI4K2A, *N*=11; (B) PI4K2B, *N*=24; (C) PI4K3A, *N*=21; and (D) PI4K3B, *N*=16 and the SE of the data in (gray) for all traces. Dashed line marks the zero-time point that was generated from individual MMP9-GFP fusion event traces (green channel) and time aligned to the red channel. Background-subtracted and normalized fluorescence intensity traces are shown for each protein.

Figure 4

Figure 5

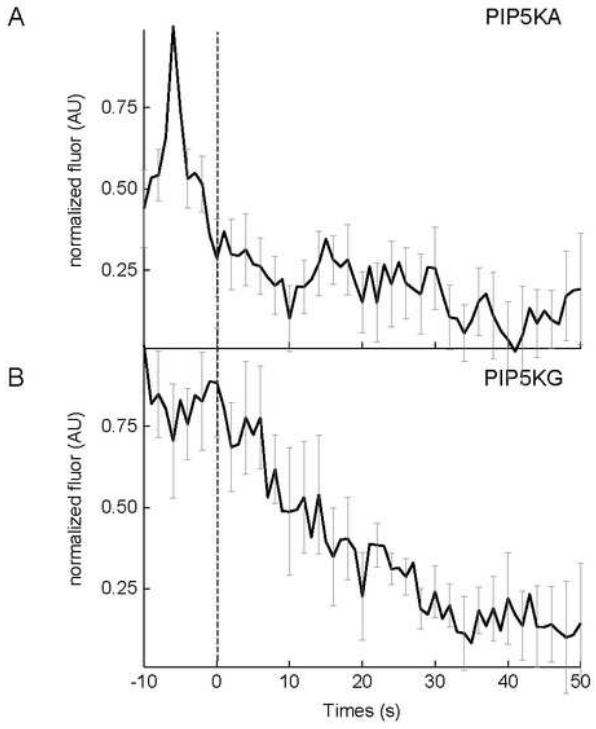

Figure 5: Average time-lapse traces of normalized fluorescence intensities signal (dark line) of red fluorescent-labeled lipid kinase isoforms, including: (A) PIP5KA, *N*=23; and (B) PIP5KG, *N*=11 and the SE of the data in (gray) for all traces. Dashed line marks the zero-time point that was generated from individual MMP9-GFP fusion event traces (green channel) and time aligned to the red channel. Background-subtracted and normalized fluorescence intensity traces are shown for each protein.

Figure 5

Figure 6

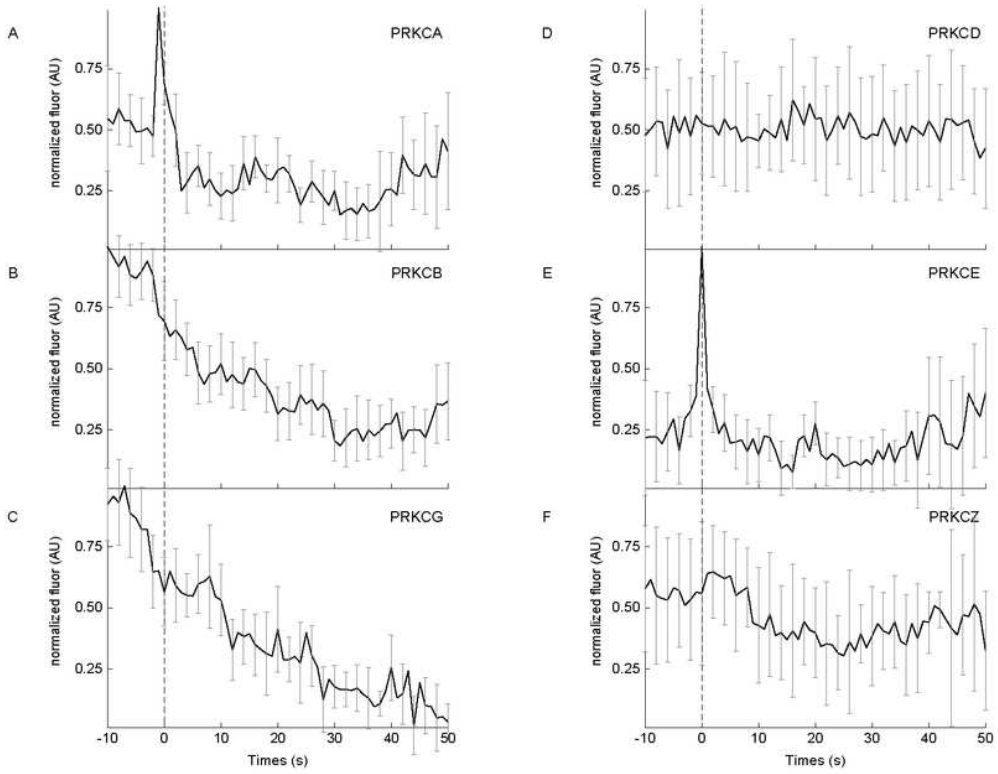

Figure 6: Average time-lapse traces of normalized fluorescence intensities signal (dark line) of red fluorescent-labeled protein kinase C isoforms, including: (A) PRKCA, *N*=25; (B) PRKCB, *N*=16; (C) PRKCG, *N*=16; (D) PRKCD, *N*=13; (E) PRKCE, *N*=25; and (F) PRKCZ, *N*=5 and the SE of the data in (gray) for all traces. Dashed line marks the zero-time point that was generated from individual MMP9-GFP fusion event traces (green channel) and time aligned to the red channel. Background-subtracted and normalized fluorescence intensity traces are shown for each protein.

Figure 6

Figure 7

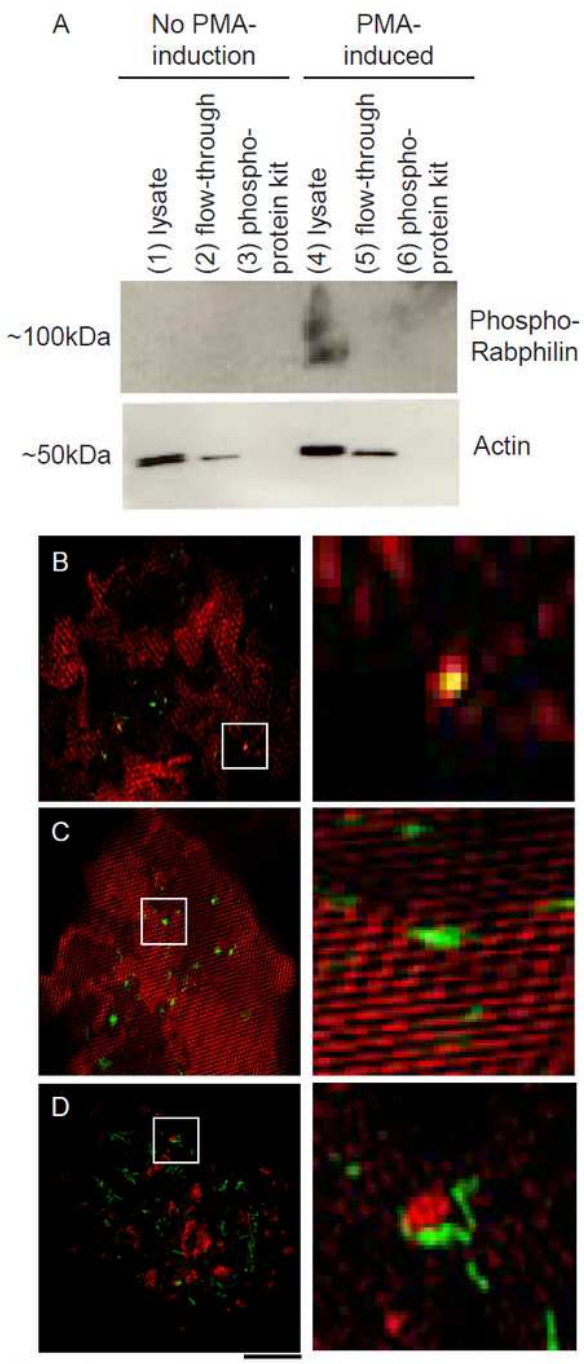

Figure 7: (A) Western blot, using unpurified lysates and various components, eluants versus concentrates, associated with phosphoprotein purification kit, for phospho-specific Rabphilin 3A (Ser234), without and with PMA-induction. Spatial organization, super resolution SIM images of PRKC isoforms with its potential phosphorylation targets during PMA induction. Shown on the left is the spatial arrangement of: (B) PRKCE with MMP9-GFP; (C) PRKCA with Rab27a; and (D) PRKCA with Rab27b. Shown on the right is the enlarged regions (boxes on left); same order as on the left.

Figure 7

Figure 8

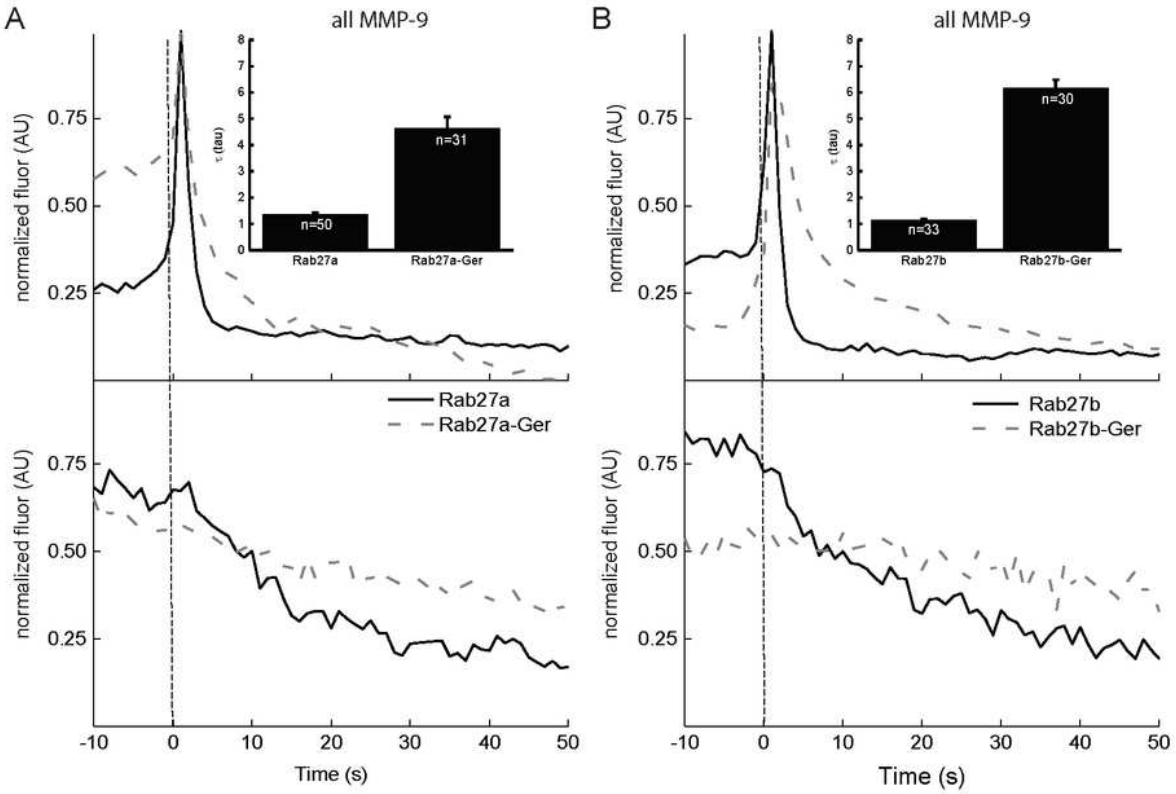

Figure 8: (A) Average time-lapse decay profiles of normalized MMP-9 fluorescence intensities (green channel; top), co-expressed with Rab27a-WT, wild-type (solid black) and Rab27a-Ger (dashed gray). The average time-lapse decay profiles of the associated normalized Rab27a-WT and Rab27a-Ger mutant fluorescence intensities (red channel; bottom) in the same MCF-7 cells is also depicted. (B) Average time-lapse decay profiles of normalized MMP-9 fluorescence intensities (green channel; top), co-expressed with Rab27b-WT (solid black) and Rab27b-Ger (dashed gray). The average time-lapse decay profiles of the associated normalized Rab27b-WT and Rab27b-Ger mutant fluorescence intensities (red channel; bottom) in the same MCF-7 cells is also depicted. Individual event traces were time-aligned to '0 s', which corresponds to the manually identified first frame of fusion.

Figure 8

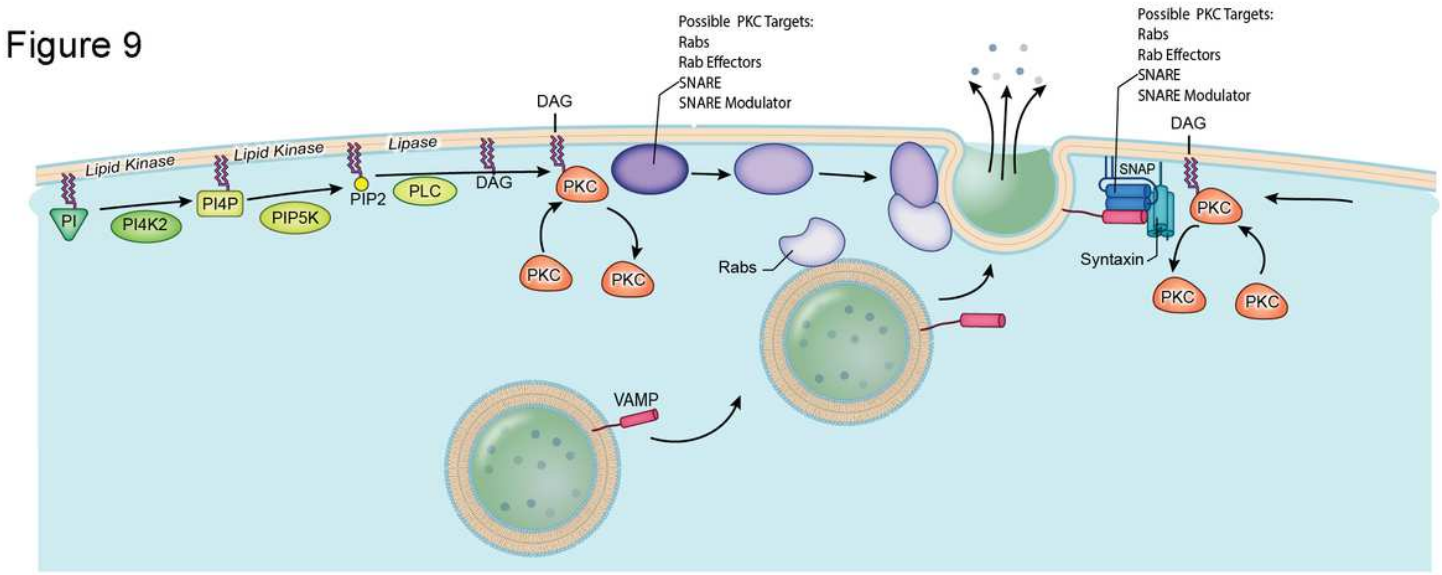

Figure 9: A depiction of the PIP2-mediated signaling pathway on the exocytosis of MMP-9 in MCF-7 cells. Illustration shows a step associated with dynamic cascade of PIP2 formation and subsequent breakdown, and the lipid kinases and protein kinases associated with exocytic sites.

Figure 9

Supplementary Files

This is a list of supplementary files associated with this preprint. Click to download.

- SupplementalLipidFigurescombined.pdf